Analysis and Synthesis of a New Class of Low Side Lobe Planar Arrays

Iqtidar Ahmad Khan

Thesis submitted to the faculty of the Virginia Polytechnic Institute and State University
in partial fulfillment of the requirements for the degree of

Master of Science
In
Electrical Engineering

Ahmad Safaai-Jazi (Chair)
Joseph B. Baker
Jeffrey H. Reed

December 20, 2017
Blacksburg, Virginia

Keywords: planar arrays, array synthesis, rectangular arrays, low side lobe planar arrays

Analysis and Synthesis of a New Class of Low Side Lobe Planar Arrays

Iqtidar Ahmad Khan

ABSTRACT

Numerical techniques for designing planar arrays with low side lobe level often require memory intensive optimization algorithms and also initialization in the form of some known values of radiation pattern parameters beforehand - information that may not be available when designing arrays. A few analytical methods exist in the literature that can be used to design rectangular lattices of isotropic elements for desired half-power beamwidth and side lobe level, but the number of elements of the array often should be known before the design process. Some array designs based on analytical techniques may suffer from severe performance limitations, an example is the uniformly excited array which cannot produce side lobe levels below −13.3 dB.

The goal of this study is to present an analytical technique for synthesis of planar arrays that, for specified radiation pattern requirements, not only provides quick solutions for the required number of elements and its distribution along the length and width of the array rectangular lattice, but also produces low side lobes without any limitation. A new class of non-uniformly excited equally spaced planar arrays is introduced and investigated in this study. The new array uses the patterns of uniformly excited linear arrays as its building blocks and has a separable element current distribution, hence making it mathematically convenient to analyze its radiation properties in terms of those of its constituent linear arrays. The proposed planar array does not suffer from the side lobe level limitation of uniformly excited planar arrays, and its synthesis, due to the analytical nature of description of its radiation properties, does not require iterative procedures that are inherent to numerical techniques.

Radiation characteristics of the proposed planar array, including directivity, side lobe level, half-power beamwidths, far-field three dimensional radiation patterns, and element excitation currents, are examined and simulation results for several example cases are

presented. The analysis culminates with successfully mapping a continuous radiation pattern to discrete element currents in a rectangular lattice geometry.

The synthesis procedure is validated by successfully designing various planar arrays with desired requirements in terms of side lobe level and half-power beamwidths in the principal planes. Several design examples are presented. Radiation characteristics of the synthesized arrays are compared with the desired design requirements which were used as input information in the synthesis process. For the cases studied, the achieved performance characteristics are close to the desired ones.

Analysis and Synthesis of a New Class of Low Side Lobe Planar Arrays

Iqtidar Ahmad Khan

GENERAL AUDIENCE ABSTRACT

A group of similar antennas that radiate with equal intensity in all directions and each fed with a certain current amplitude is called an isotropic antenna array. When the distance between the adjacent antenna elements in an array is constant, it is called an equidistant array. Furthermore, when the array elements take up the geometry of a rectangular lattice, they are referred to as rectangular planar array.

In antenna array design, it is always desirable that the isotropic array is set up in a manner that it establishes a stronger communication link in the desired direction while minimizing any communication in other directions. This can be achieved by changing the spatial footprint of the array's radiation also known as its array factor. The array factor can be altered by either adjusting the inter-element spacing or changing the current amplitude of each element.

A great number of techniques have been proposed over the years that aim to minimize communication in undesired directions. Most of these techniques achieve the objective by employing computationally complex algorithms that require a lot of time and memory. For other synthesis techniques, some design information is required to be known beforehand which may not be possible.

The aim of this study is to present an easier analytical approach that designs rectangular planar array for specified radiation pattern requirements. The radiation requirements entail the direction in which the communication link is required to be established and the extent to which radiation in other directions is permissible – characterized by side lobe level of the array factor. The strength of the communication link is measured by directivity and half power beam width of the array factor. It is found that the proposed array in the study minimizes communication in unwanted directions in a much more effective manner than a

rectangular array with each element fed with an equal current amplitude – also known as uniformly excited planar array.

The performance of the proposed planar array in terms of directivity, half power beam width and side lobe level is first simulated and presented. The design procedure is then validated by designing various planar arrays with desired radiation requirements. Several design examples are presented. Radiation characteristics of the synthesized arrays are compared with the desired design requirements which were used as input information in the synthesis process. For the cases studied, the achieved performance characteristics are close to the desired ones.

To my mother Ghazala Khan, my father Abdul Qadir

To my brothers Abrar Khan and Gohar Salim

and my sister Rehana Khan

ACKNOWLEDGEMENTS

I would like to thank my academic advisor Dr. Ahmad Safaai-Jazi for his mentorship throughout the course of this study. He provided all the theoretical framework that laid the foundation of this research study. I am particularly grateful for his dedication and time without which this study was not possible. I also appreciate the patience with which he combed through the entire simulation code with me and in the process improved my attention to detail. The courses he offered also played an instrumental role in motivating me to pursue the project.

I am also thankful to Dr. Joseph Baker for his guidance and support especially during my early days at VT and for taking out time to review my thesis and providing valuable feedback. I would also like to extend my gratitude to Dr. Jeffery Reed for agreeing to be in my thesis committee and for his useful comments.

I would like to thank Jennifer Dsouza for all her moral and emotional encouragement throughout this time and for carrying donuts and coffee to my Thesis Defense. I am also grateful to Asad Ullah Khan for being a friend in need and Xavier Gomez, for all the intellectually stimulating conversations. Their friendship enriched my academic and personal journey at VT.

I also wish to thank my family for their motivation and support. My mother, Ghazala Khan for inspiring me through her perseverance and her willingness to sacrifice everything for her children. My father, Abdul Qadir Khan for encouraging me to pursue graduate studies, my siblings Rehana Khan and Abrar Khan for bearing my rants and lastly, Gohar Salim for being there through thick and thin. I couldn’t have made it this far without them.

Table of Contents

List of Figures

List of Tables

Chapter 1: Introduction

1.1 Background

Antenna arrays have existed for decades with applications spanning defense, cellular communications, and metrology to name a few. From the X-band radar detecting incoming missiles in Aegis missile defense systems to base stations (BSs) that connect millions of users each day, all employ antenna arrays that lay down the desired electromagnetic footprint. The desired electromagnetic footprints also known as the radiation patterns are crucial to the realization of intended applications of the arrays.

Mobile communication remains one area of application of antenna arrays that is evolving rather rapidly [1]. With the increase in data traffic, more usage of smart phones and demand for higher data rates, it has become inevitable to foresee a future where more users are interconnected using mm-wave band, a spectrum that so far remains largely untapped [2].

Many studies already suggest that the future 5G system would include greater number of base stations to cover the same physical area owing to the high attenuation in mm-wave propagation. The 5G architecture only seems plausible with large number of BSs placed close to each other and equipped with highly directive antenna arrays. Some experiments conducted in New York City already suggest that the distances between BSs could shrink to as short as 1.7 km [3]. Furthermore, work has already begun on designing antennas and array configurations that would be the most suitable for 5G mobile communications [4].

With more reliance on mm-wave communications and the subsequent changes in the antenna architecture to support such communication systems in the future, it is all the more important to revisit existing backend array design techniques and come up with simpler novel solutions. Innovation in array modeling techniques is also particularly important as it is the first step in the design process that eventually culminates into hardware production, and having simpler backend design techniques would assist in the overall design process.

1.2 Literature Survey

Planar arrays have a wide range of applications. Discrete elements placed in a planar configuration have already been used in satellite communications [5], so are 4000

slots fed by 28 waveguides in planar arrangement for phased array scanning in Airborne Warning and Control System (AWACS). Rectangular lattice arrays are also used for three dimensional (3-D) acoustic imaging in medical applications [6]. The low profile and greater agility of these arrays make them extremely useful for such applications. Furthermore, the array factor of planar arrays is a function of both the elevation and azimuth angles, thus these arrays provide greater resolution in both angular directions [7].

A Planar array can be characterized according to the geometry of its lattice. Some commonly used configurations of planar arrays are depicted in Figure 1.1 (a) – (c) in which all array elements are identical. Figure 1.1 (a) represents a class of planar arrays known as circular array. The array elements are arranged in concentric circles and each element on any given circle, c_x, is distance r_x away from the origin. Each circle in Figure 1.1 (a) also represents a circular array and the overall geometry can be regarded as an array of circular arrays. The array configuration in Figure 1.1 (b) illustrates non-uniformly spaced planar array in which the distance between adjacent elements is not equal. This class of array is also referred to as sparse array.

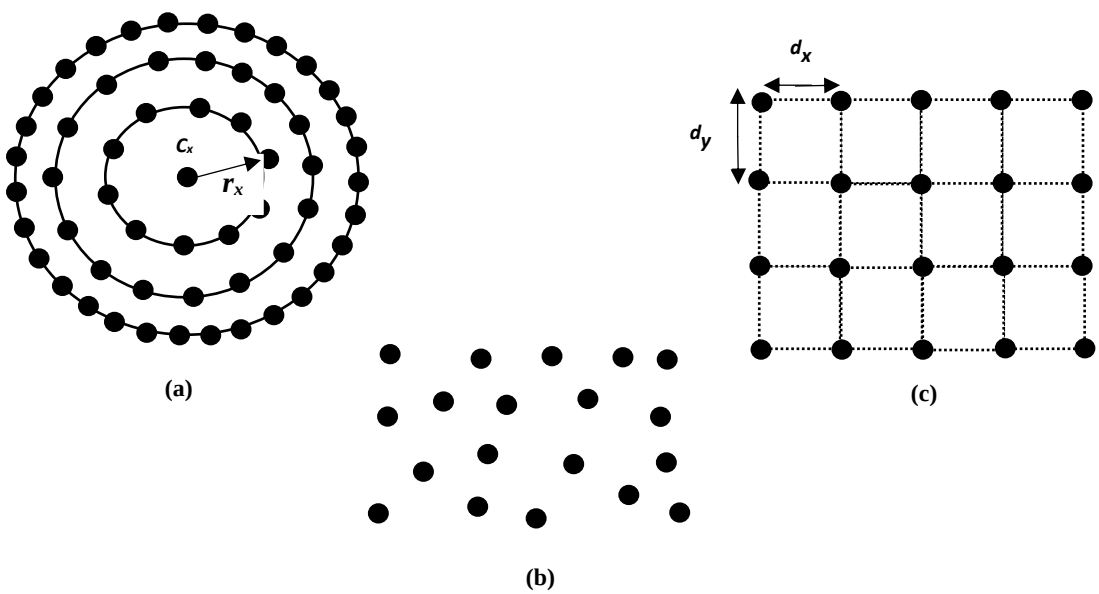

Figure 1.1: geometries of (a) circular planar arrays, (b) sparse planar array, (c) uniformly spaced planar array

The arrangement in Figure 1.1 (c) depicts the geometry of a uniformly spaced planar array. For uniformly spaced planar arrays, the distance between consecutive array elements (d_x or d_y) placed along either cardinal direction is equal. If $d_x = d_y$, the geometry takes the form of a square planar array. When $d_x \neq d_y$ the lattice is referred to as rectangular planar array.

Over the years, a mix of both analytical and numerical techniques have been proposed for planar array synthesis. These methods have aided in the design of the above mentioned array geometries for various applications. The arrays placed in two dimensions have been designed to not only achieve the desired radiation characteristics such as half-power beamwidth, directivity, nulls, side lobe level, etc., but also to do so in the simplest and most efficient manner.

The radiation characteristic requirements vary with applications, hence rendering some design techniques more desirable than others. The synthesis techniques reported in the literature have been driven by various motivations. While some planar array synthesis techniques have tried to address the issues of increasing cost and hardware complexity of the feed structure, others, to a varying extent, have strived to realize the desired radiation pattern characteristics. These various techniques are discussed in some detail before a new design approach is suggested.

The dominating theme in the literature of planar array synthesis has mostly revolved around reducing the array size. That is because reducing the number of active array elements in any geometrical configuration, circular, linear, or rectangular, reduces the cost and simplifies the feed system [8]. Also, challenges with implementing amplitude tapering or non-uniform excitations [9] have provided further impetus to view the planar array synthesis problem as an ‘array thinning’ task requiring optimization, whereby the number of array elements in a lattice is reduced from an initial number until the desired radiation pattern is achieved.

The aim to conserve cost and simplify feed hardware in the design process has led to the proposal of a different class of arrays called aperiodic or sparse planar arrays. They are non-uniformly placed arrays or, in other words, planar arrays with variable inter-element spacing between neighboring elements. Sparse arrays have mostly been designed using

numerical optimization techniques, hence generating considerable interest in various types of iterative techniques to solve the problem [10].

The focus on numerical techniques owes to the nonlinear nature of the problem. The array factor for an aperiodic planar array is a nonlinear function of the inter-element distance. The existence of infinite number of possible positions that may give a pattern close to the desirable pattern have further added to the difficulty in finding the right configuration [11]. Since no unique solution exists, it is hard to come up with analytical expressions for sparse planar array synthesis.

Most numerical procedures have aimed at optimizing the position of each element in a planar array to realize the desirable radiation characteristics such as side lobe level, half-power beam width, gain, etc. and that too with the least number of elements. These optimization methods could be classified into two categories: One that involves turning individual elements 'on' or 'off' while keeping the element positions unchanged [12]. The second achieves optimization by perturbing the positions of the array elements [13].

While numerical synthesis methods, to varying degrees of success, have resulted in practical configurations of planar arrays, they have had their share of limitations and challenges. As discussed earlier, due to the lack of closed form solutions, the whole process of implementing numerical algorithms involves a large number of iterations and programming techniques. The process is time and memory consuming, and more so as the number of array elements increases. What makes the optimization process further challenging is the possible presence of minima in the cost function, complicating the convergence of the iterative process. Furthermore, most of the iterative procedures require initial information of radiation characteristics, which have to be close to the final pattern characteristics, something not known beforehand. Hence, further making it harder for the iterative process to converge.

Since the direction of arrival of signal and interference is unknown, it is always desirable in array design to have a flexible, steerable main lobe and nulls to maximize signal extraction and minimize interference. However, many of the optimization techniques have only worked for a fixed boresight directions and the scanning problem is not addressed [14].

Other optimization techniques have been proposed to accommodate arbitrary boresight directions [15]. This means optimizing a different set of possible solutions whenever the boresight direction changes in elevation and azimuth angular coordinates. With each sparse planar array arrangement different for a different boresight case, it becomes quite impractical to vary the inter-element distance every time the radiation pattern requirements change. Furthermore, running computer routines every time the beam pattern requirements change also takes a toll on computer memory and causes undesirable time delays.

Optimization techniques have also been employed on the phase of equally spaced planar arrays with constant excitations to reduce side lobe level [16]. However, like the amplitude tapered arrays, the challenge with the synthesis of planar arrays by this method is lowering of directivity once the side lobe level is minimized. Even though analytical approximations give acceptable syntheses, they are still not as accurate as numerical results which, like sparse planar array optimization, require a lot of memory.

Other than numerical optimization methods, few analytical techniques have also been proposed in the literature for synthesis of planar arrays which can be attributed to the inherent mathematical difficulty in finding the inverse function that maps the continuous two parameter dependent array factor function to finite discrete element excitation coefficients. The constraints on the geometrical boundaries of array elements further complicates the synthesis problem [17].

Analytical techniques have mostly been used to design equally spaced planar arrays with rectangular or square lattice configurations. The most common procedure to design rectangular planar arrays has been based on the array factor being equal to the multiplication of the array factors of two linear one dimensional arrays placed orthogonal to each other [18]. These techniques are usually referred to as the synthesis approach using separable distributions.

Radiation patterns achieved using separable distributions have their highest level side lobes in the principal planes whereas those outside the principal planes are significantly lower. This is because the side lobes in the principal planes are those of the linear array patterns while those outside the planes are the product of the side lobes of individual linear arrays.

This is a significant issue when the design requires the side lobes with maximum level to be placed outside a principal plane.

Other analytical techniques can be classified as non-separable synthesis methods. The work of Tseng and Cheng [20] forms the basis of such techniques. The proposed analytical procedure in this study builds on [19] and provides current distributions for square planar arrays that produce the required beam pattern. Non-separable analytical techniques have garnered a lot of attention because they provide much more flexibility in controlling the side lobe topography. The approach used in [20] was extended by Collins [21] to rectangular arrays and produced lower side lobes in the principal planes and higher elsewhere. Researchers have used these analytical expressions to define new classes of equally spaced square arrays known as modified Chebyshev and Bessel planar arrays [22] and [23]. The work presented in [20], [21], and [22] provide equal side lobes for any cross section, making the procedure akin to Dolph-Chebyshev procedure for planar arrays.

The synthesis procedures employed in [20], [22], and [23] yield analytical expressions for the array factor, half-power beamwidth, directivity and element excitation coefficients. However, these synthesis procedures require the information on the number of elements to be known beforehand which may not be possible every time. Furthermore, these methods only allow synthesis of square lattices of array elements. A significant limitation of uniformly excited arrays is that they cannot provide side lobe levels lower than -13.3 dB which may not be adequate for many applications [24]. Also, Chebyshev arrays suffer from directivity saturation and very large current taper ratio when the number of elements become large.

The aim of this research is to introduce new planar array designs which would allow desirable side lobe level below -13.3 dB to be achieved and also alleviate the problems associated with Chebyshev designs. Analysis of the radiation characteristics of the proposed new arrays is presented, then a synthesis procedure is developed which yields the number of required elements and their excitation currents in order to meet specified design requirements.

1.3 Scope of the Proposed Research

A new analytical technique for synthesis of low side lobe planar arrays is proposed in this study. It makes use of the array factor of a uniformly excited equally spaced planar array to form a nonuniformly excited array which meets specified design requirements. A significant advantage of this synthesis technique is that analytical expressions for quick calculation of element excitation currents are obtained and it also allows considerable control over side lobe level, half-power beamwidths, and boresight direction. These arrays are a product of nonuniformly excited equally spaced linear arrays discussed in [24] and belong to the class of planar arrays with separable distributions [25]. The radiation properties of the new arrays introduced are closely linked to those of their linear components and can be analyzed by studying the array factors of the constituent linear arrays.

Chapter 2 presents the theoretical developments of the array factor for the proposed new arrays using the separable distribution technique. An inverse function is determined that successfully maps continuous array factor to the discrete elements having specific excitations. This synthesis procedure leads to analytical, compact, closed form solutions for the array factor from which all radiation characteristics including directivity, half-power beamwidths, side lobe level, and element excitation currents can be determined. The analytical relationships governing the radiation properties of the proposed arrays are developed in the same manner as that used for linear one-dimensional arrays discussed in [24]. Three principal equations, one for the side lobe level and two for half-power beamwidths, are derived using three design requirements of the array.

The behavior of these equations is simulated and analyzed for various design parameters in Chapter 3. The extent to which each design parameter influences the side lobe level and the two half-power beamwidths of the proposed arrays is tabulated, plotted and analyzed. The numerical results in Chapter 3 are used to validate the theoretical observations made on the radiation characteristics examined in Chapter 2.

Chapter 4 uses the expressions developed in Chapter 2 for synthesis of arrays with specified design requirements. The synthesis is achieved by solving the three principal equations, describing the side lobe level and the two half-power beamwidths, simultaneously to

determine the three design parameters. The three design parameters are used to find the number of elements and calculate the excitation coefficients of the array which are then used to determine the radiation pattern. In order to verify that the synthesis technique indeed meets the desired requirements, the calculated array factor is simulated and the actual side lobe level as well as the half power beamwidths that the designed array can produce are determined and verified.

Chapter 5 proposes future work that lies within the scope of this new class of arrays. The most important of which are designing arrays with limited current taper ratios and considering the effects of mutual coupling among the elements in order to determine the radiation properties under more realistic conditions and make the design more practical in certain applications. The type of antenna element used to achieve the proposed array design would also influence the performance of the array and its radiation properties need be accounted for.

Chapter 2: Theoretical Developments

In this chapter the theoretical framework for the analysis of radiation characteristics of a new class of planar arrays, referred to as Low Sidelobe Planar Arrays (LSPA), is presented. The array factor of the proposed planar arrays is formulated and used to determine their radiation properties including side lobe level (SLL), half-power beamwidth (HPBW), directivity (D), and the element excitation currents. The formulation developed here is also employed later in synthesizing planar arrays with prescribed pattern characteristics such as side lobe level and half-power beamwidths. The constraints under which the synthesis procedure remains valid are also examined.

2.1 Geometry, Coordinates, and Parameters

Figurers 1a and 1b illustrate the geometry and angular coordinates used in developing the mathematical description of the new two-dimensional planar array introduced in this work. The array consists of N_x x N_y identical elements with their centers lying on the *xy*-plane and forming a rectangular grid as shown in Fig. 1a. The elements are assumed to have the same spatial orientation so that all have the same far-field radiation pattern and the same polarization. Furthermore, the elements are equally spaced in both *x* and *y* directions, with element spacings d_x and d_y along the *x*- and *y*-axes, respectively. The spherical polar coordinates θ and φ are used to define an arbitrary direction in space along a line passing through the origin, labelled *r*, as shown in Fig. 1b. The three-dimensional radiation patterns of arrays are described in terms of these two angles through the array factor AF(θ, φ). Two other angles, denoted as θ_x and θ_y, greatly facilitate the formulation of the array factor for planar arrays. θ_x is the angle between the *x*-axis and line *r*, while θ_y is the angle between the *y*-axis and line *r*. The relationships between θ_x and θ_y and the polar coordinates θ and φ are given by equations (2.1) and (2.2).

$$\cos\theta_x = \sin\theta\cos\phi \tag{2.1}$$

$$\cos\theta_y = \sin\theta\sin\phi \tag{2.2}$$

It is emphasized that the three angles θ, θ_x, and θ_y vary between 0 and 180 degrees, whereas the angle φ varies between 0 and 360 degrees. In addition to four variable angles

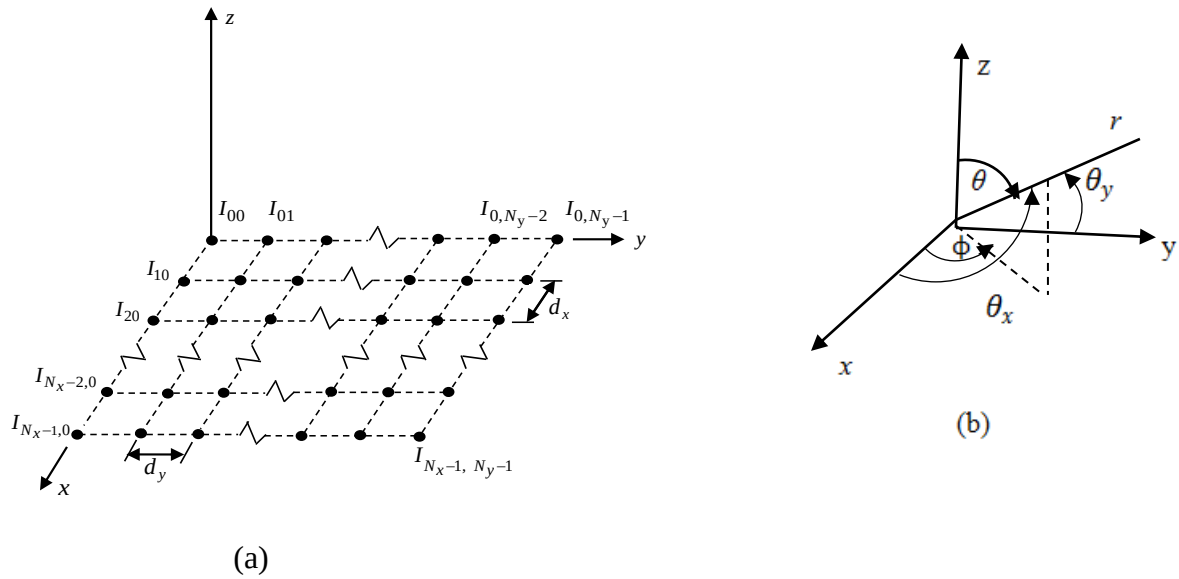

Figure 2.1 (a) Geometry of a rectangular planar array with equal element spacings in the *x* and *y* directions, (b) angular coordinates used in describing the array factor

θ, φ, θ_x, and θ_y , four constant angles, denoted as θ_0, φ_0, θ_{0x}, and θ_{0y}, are also used to describe the direction along which the maximum radiation occurs. The latter two angles in terms of θ_0 and φ_0 are given as

$$\cos\theta_{0x} = \sin\theta_0 \cos\phi_0 \tag{2.3}$$

$$\cos\theta_{0y} = \sin\theta_0 \sin\phi_0 \tag{2.4}$$

2.2 Development of Array Factor

In order to prepare the ground for the development of the array factor for planar arrays that are the subject of investigation in this thesis, first the array factor of a uniformly excited, equally-spaced linear array is reviewed. Array factor is defined by IEEE as the radiation pattern when each array element is considered to radiate isotropically [26]. Considering a linear array with *n* elements along the *z*-axis and with element spacing *d*, its array factor can be expressed as [27]

$$f(\psi) = \frac{\sin\left(\frac{n\psi}{2}\right)}{n\sin\left(\frac{\psi}{2}\right)} \tag{2.5}$$

where $\psi = \left(\frac{2\pi d}{\lambda}\right)(cos\theta - cos\theta_0)$, λ is the wavelength, θ the elevation angle measured from the z-axis and $\theta = \theta_0$ is the angle of the maximum radiation intensity. It is worth noting that the array factor in (2.5) assumes its maximum value of unity at ψ=0, is a periodic function of ψ with a period of 2π, and has even symmetry about ψ=±2kπ, k=0,1, 2, …. Furthermore, $f(\psi)$ processes nulls at ψ=±2π/n, ±4π/n, …, ±2π(1−1/n). The array factor for a uniformly excited planar array, as that shown in Fig. 1a, can be readily determined using the result in (2.5). This is done by considering the linear arrays in the y-direction as elements of an array in the x-direction and using the principle of pattern multiplication. Accordingly, the array factor for the uniformly excited planar array with n_x x n_y elements is expressed as

$$f_{xy}(\psi_x, \psi_y) = f_x(\psi_x) \cdot f_y(\psi_y) = \frac{\sin\left(\frac{n_x\psi_x}{2}\right)}{n_x \sin\left(\frac{\psi_x}{2}\right)} \cdot \frac{\sin\left(\frac{n_y\psi_y}{2}\right)}{n_y \sin\left(\frac{\psi_y}{2}\right)} \tag{2.6}$$

where

$$\psi_x = \left(\frac{2\pi d_x}{\lambda}\right)(cos\theta_x - cos\theta_{0x}) = \left(\frac{2\pi d_x}{\lambda}\right)(\sin\theta\cos\phi - \sin\theta_0\cos\phi_0) \tag{2.7}$$

$$\psi_y = \left(\frac{2\pi d_y}{\lambda}\right)(cos\theta_y - cos\theta_{0y}) = \left(\frac{2\pi d_y}{\lambda}\right)(\sin\theta\sin\phi - \sin\theta_0\sin\phi_0) \tag{2.8}$$

It is well known that uniformly excited linear as well as planar arrays cannot provide side lobe levels lower than − 13.3 dB which may not be adequate for many applications [24, 28]. The principal aim of this research is to introduce planar array designs which would allow desirable side lobe level below −13.3 dB without any limitation. To achieve this goal, an approach similar to that used for reducing the side lobe level in linear uniformly excited arrays is employed. In doing so, a non-uniformly excited planar array is formed such that its array factor is set equal to the array factor of a uniformly excited planar array raised to m^{th} power. That is,

$$AF(\psi_x, \psi_y) = \left|\frac{\sin\left(\frac{n_x\psi_x}{2}\right)}{n_x \sin\left(\frac{\psi_x}{2}\right)} \cdot \frac{\sin\left(\frac{n_y\psi_y}{2}\right)}{n_y \sin\left(\frac{\psi_y}{2}\right)}\right|^m \tag{2.9}$$

Clearly, by properly choosing the value of m >1 side lobe levels at any desired level below −13.3 dB can be achieved. It is emphasized that m is a real number which may be integer or non-integer. The array factor in (2.9), when $m \neq 1$, represents a nonuniformly excited planar array which will be used to determine the radiation properties of the array and its element excitation currents as discussed in the following sections.

2.3 Analysis of Side Lobe Level

2.3.1 Side Lobe Level of Non-uniformly Excited Linear Arrays

The side lobe level (SLL) of an array is defined as the second highest peak of the array factor which is usually located in the vicinity of the main lobe of radiation pattern. As will be noted later, the side lobe level of the proposed planar arrays is closely related to the side lobe level of their constituent non-uniformly excited linear arrays (NUELA) whose array factor is the mth power of the right-hand-side expression in (2.5). Assuming that the second highest peak occurs at $\psi = \psi_{SLL}$, SLL in dB for NUELA is obtained from

$$SLL_{dB} = 20\log_{10}\left|\frac{\sin\left(\frac{n\psi_{SLL}}{2}\right)}{n\sin\left(\frac{\psi_{SLL}}{2}\right)}\right|^{m} \tag{2.10}$$

When $n = 2$, no side lobes exist and they only start appearing when $n \geq 3$. It has been shown in [24] that when $n \geq 3$, the SLL point ψ_{SLL} in $f(\psi)$ function is the same for all values of m and lies in the range $\frac{2\pi}{n} \leq \psi \leq \frac{4\pi}{n}$, in the neighborhood of $\frac{3\pi}{n}$. Figure 2.2 shows the array factor variations in the $\frac{2\pi}{n} \leq \psi \leq \frac{4\pi}{n}$ region. The SLL point, ψ_{SLL}, on the ψ-axis for $n = 5, d = \frac{\lambda}{2}$ remains 1.817 for $1 \leq m \leq 4$. Therefore, ψ_{SLL} of a uniformly excited linear array described by (2.5) can be determined and then used in (2.10) to calculate the SLL for NUELA for known values of m.

A design equation that approximates the ψ_{SLL} point for a design parameter n is obtained in [24]. It is developed by considering a Taylor series approximation of the array factor in (2.5) at $\psi = \psi_0 = \frac{3\pi}{n}$ and is given as follows

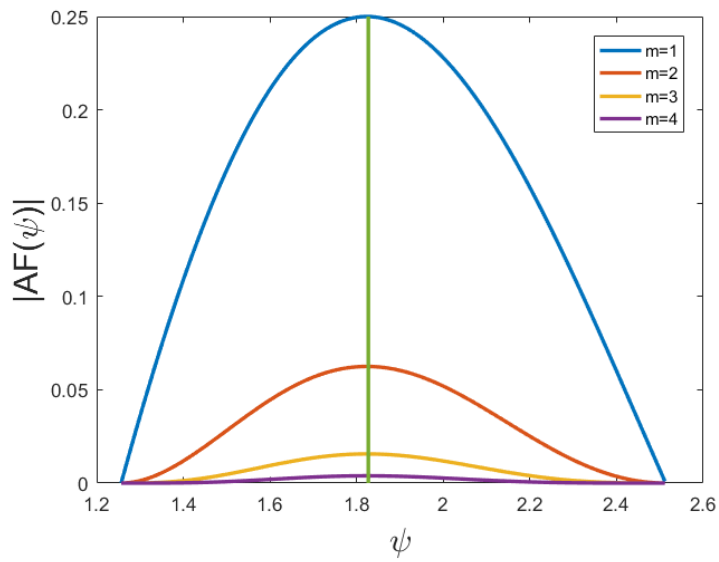

Figure 2.2: The side lobe with second largest peak for arrays with *n*=5, $\boldsymbol{d = \frac{\lambda}{2}}$, $\boldsymbol{1 \leq m \leq 4}$

$$\psi_{SLL} = \psi_0 - \frac{\sin(\psi_0)}{(n^2+1)\sin^2\left(\frac{\psi_0}{2}\right) - 2}, \qquad \psi_0 = \frac{3\pi}{n} \tag{2.11}$$

2.3.2 SLL of Low Side Lobe Non-uniformly Excited Planar Arrays

The SLL of the proposed array is established by examining the SLL of its constituent NUELAs whose array factors are given as

$$AF_x(\psi_x, n_x) = \left| \frac{\sin\left(\frac{n_x \psi_x}{2}\right)}{n_x \sin\left(\frac{\psi_x}{2}\right)} \right|^m \tag{2.12}$$

$$AF_y(\psi_y, n_y) = \left| \frac{\sin\left(\frac{n_y \psi_y}{2}\right)}{n_y \sin\left(\frac{\psi_y}{2}\right)} \right|^m \tag{2.13}$$

Comparison of (2.12) and (2.13) with (2.10) implies that the peak of the largest side lobe for $AF_x(\psi_x, n_x)$ occurs when $\psi_x = \psi_{SLL}^x$ and for $AF_y(\psi_y, n_y)$ when $\psi_y = \psi_{SLL}^y$, where

$$\psi_{SLL}^{x} = \psi_{0x} - \frac{\sin(\psi_{0x})}{(n_x^2+1)\sin^2\left(\frac{\psi_{0x}}{2}\right) - 2}\ , \psi_{0x} = \pm\frac{3\pi}{n_x} \tag{2.14}$$

$$\psi_{SLL}^{y} = \psi_{0y} - \frac{\sin(\psi_{0y})}{(n_y^2+1)\sin^2\left(\frac{\psi_{0y}}{2}\right) - 2}\ , \psi_{0y} = \pm\frac{3\pi}{n_y} \tag{2.15}$$

It can be further stated that larger of the side lobes of the two linear arrays determines the SLL of the proposed planar array. The larger values of n_x and n_y results in smaller values of ψ_{SLL}^{x} and ψ_{SLL}^{y} in (2.14) and (2.15) and lower values of $AF_x(\psi_{SLL}^{x}, n_x)$ and $F_y(\psi_{SLL}^{y}, n_y)$. This means that when $n_x < n_y$, $AF_x(\psi_{SLL}^{x}, n_x) > AF_y(\psi_{SLL}^{y}, n_y)$. Thus, when $\psi_y = 0$, $AF_y(\psi_{SLL}^{y}, n_y) = 1$ and $\psi_x = \psi_{SLL}^{x}$ in $AF_x(\psi_{SLL}^{x}, n_x)$ defines the SLL of the total array factor. Likewise for $n_x > n_y$, $AF_x(\psi_{SLL}^{x}, n_x) < AF_y(\psi_{SLL}^{y}, n_y)$ and $\psi_x = 0$ with $\psi_y = \psi_{SLL}^{y}$ defines the SLL of the total array factor. In summary, the SLL in dB of the proposed planar array can be computed by first determining *n* and ψ_{SLL}according to the relationships in (2.16) and (2.17) and then using them in (2.10).

$$n = \begin{cases} n_x\ , & n_x < n_y \\ n_y\ , & n_x > n_y \end{cases} \tag{2.16}$$

$$\psi_{SLL} = \begin{cases} \psi_{SLLx}\ , & n_x < n_y \\ \psi_{SLLy}\ , & n_x > n_y \end{cases} \tag{2.17}$$

2.3.3 Validity of Side Lobe Level

To make sure that the SLL of the total array factor can indeed be determined as discussed above, it is necessary to show that $\psi_x = \psi_{SLL}^{x}$ and $\psi_y = 0$ for $n_x < n_y$, or $\psi_y = \psi_{SLL}^{y}$ and $\psi_x = 0$ for $n_x > n_y$, provide real values for θ and ϕ at which the side lobe level is found. Therefore, continuing for $n_x > n_y$, we have

$$\psi_y = 0 \rightarrow \left(\frac{2\pi d_y}{\lambda}\right)(\cos\theta_y - \cos\theta_{0y}) = 0 \rightarrow \cos\theta_y = \cos\theta_{0y}$$

or

$$\sin\theta\sin\phi = \sin\theta_0\sin\phi_0 \tag{2.18}$$

Also,

$$\psi_x = \psi_{SLL}^x \rightarrow \left(\frac{2\pi d_x}{\lambda}\right)(\cos\theta_x - \cos\theta_{0x}) = \psi_{SLL}^x$$

or

$$\cos\theta_x = \sin\theta\cos\phi = \psi_{SLL}^x\left(\frac{\lambda}{2\pi d_x}\right) + \underbrace{\cos\theta_{0x}}_{\sin\theta_0\cos\phi_0} \tag{2.19}$$

Dividing (2.18) by (2.19), yields

$$\tan\phi = \frac{\sin\theta_0\sin\phi_0}{\psi_{SLL}^x\left(\frac{\lambda}{2\pi d_x}\right) + \cos\theta_{0x}} \tag{2.20}$$

Squaring (2.18) as well as (2.19) and adding them gives (2.21)

$$\sin^2\theta\left(\underbrace{\sin^2\phi + \cos^2\phi}_{=1}\right) = \sin^2\theta_0\sin^2\phi_0 + \left[\psi_{SLL}^x\left(\frac{\lambda}{2\pi d_x}\right) + \cos\theta_{0x}\right]^2$$

$$\sin\theta = \left\{\sin^2\theta_0\sin^2\phi_0 + \left[\psi_{SLL}^x\left(\frac{\lambda}{2\pi d_x}\right) + \cos\theta_{0x}\right]^2\right\}^{\frac{1}{2}} \tag{2.21}$$

Examination of (2.20) indicates that a real value of ϕ will always exist for all $0 \le \theta_0 \le 180$, $0 \le \phi_0 \le 360$ and for all ψ_{SLL}^xdefined for $n_x \ge 3$, because $-\infty \le \tan\phi \le \infty$. However, (2.21) reveals that for θ to exist as a real angle, it is necessary that $\sin\theta \le 1$, or

$$\underbrace{\sin^2\theta_0\sin^2\phi_0}_{\cos^2\theta_{0y}} + \left[\psi_{SLL}^x\left(\frac{\lambda}{2\pi d_x}\right) + \cos\theta_{0x}\right]^2 \le 1$$

or

$$\left[\psi_{SLL}^x\left(\frac{\lambda}{2\pi d_x}\right) + \cos\theta_{0x}\right]^2 \le 1 - \cos^2\theta_{0y} = \sin^2\theta_{0y}$$

$$\left|\psi_{SLL}^x\left(\frac{\lambda}{2\pi d_x}\right) + \cos\theta_{0x}\right| \le \sqrt{1 - \sin^2\theta_0\sin^2\phi_0} \tag{2.22}$$

When $\theta_0 = 0°$ (2.20) yields $\tan\phi = 0$, thus $\phi = 0°$ or $180°$. Moreover, from (2.21), $\sin\theta = \left|\psi_{SLL}^x\left(\frac{\lambda}{2\pi d_x}\right)\right| = |\cos\theta_x| \le 1$ so condition (2.21) is also satisfied. Thus, when $\theta_0 = 0°$, as long as SLL is not influenced by the grating lobe and n_x & $n_y \ge 3$, the method of calculation of SLL outlined above yields the correct answer. When $\theta_0 > 0°$, (2.22) should be satisfied for $n_x < n_y$. When $n_x > n_y$, the required condition is

$$\left|\psi_{SLL}^{y}\left(\frac{\lambda}{2\pi d_y}\right)+\ \sin\theta_0\sin\phi_0\right|\leq\sqrt{1-\sin^2\theta_0\sin^2\phi_0} \tag{2.23}$$

2.4 Calculation of the Half-Power Beamwidth

2.4.1 Half-Power Beamwidth of NUELA

The HPBW of a radiation pattern defines the angle between two points on the main lobe at which the radiation intensities are one half the value along the direction of maximum radiation. For a linear array, the half-power points denoted as $\pm\psi_{HP}$ satisfy the following relationship

$$|AF(\pm\psi_{HP})|=\frac{1}{\sqrt{2}} \tag{2.24}$$

When both half-power points are in the visible region, $\pm\psi_{HP}$ in terms of elevation angles at half-power points, $\theta_{HP,right}$ and $\theta_{HP,left}$, are expressed as

$$\psi_{HP}=\frac{2\pi d_x}{\lambda}(\cos\theta_{HP,right}-\cos\theta_0) \tag{2.25}$$

$$-\psi_{HP}=\frac{2\pi d_x}{\lambda}(\cos\theta_{HP,left}-\cos\theta_0) \tag{2.26}$$

Then, the half-power beamwidth is computed as

$$HPBW=\ \left|\theta_{HP,left}-\theta_{HP,right}\right| \tag{2.27}$$

An alternative analytical expression defining the half power point, ψ_{HP}, in terms of the half power beam width HPBW, boresight direction θ_0, wavelength λ and the inter-element spacing d, was derived for NUELA in [24] and is given in (2.28).

$$\psi_{HP}=\frac{2\pi d}{\lambda}\tan\left(\frac{HPBW}{2}\right)\sqrt{\cos^2\left(\frac{HPBW}{2}\right)-\cos^2\theta_0} \tag{2.28}$$

2.4.2 HPBW of Low Side Lobe Non-uniformly Excited Planar Arrays

In linear arrays, because of the rotational symmetry of the radiation pattern about the z-axis only one half-power beamwidth in a plane containing the z-axis is defined. In planar arrays, however, two beamwidths in two principal planes are defined. When the

direction of maximum radiation on the main beam of the array pattern is along the z-axis; that is $\theta_0 = 0°$, the principal planes are considered to be *xz*- and *yz*-planes. However, when the peak radiation on the main beam is along an arbitrary direction $(\theta_0 \neq 0°, \varphi_0)$, *xz*- and *yz*-planes are not suitable for half-power beamwidth analysis. The principal planes used for the calculation of beamwidths of planar arrays studied here are *x*-*r* and *y*-*r* planes. The *x*-*r* plane comprises the *x*-axis and the radial line going through the origin along the main beam maximum that is defined by θ_0 and ϕ_0 . Similarly, the *y*-*r* plane is made of *y*-axis and the same radial line mentioned above. The half-power points determining $HPBW_x$ and $HPBW_y$, on the *x*-*r* and *y*-*r* planes must satisfy (2.29) and (2.30) respectively.

$$\left|\frac{\sin\left(\frac{n_x\psi_{HPx}}{2}\right)}{n_x\sin\left(\frac{\psi_{HPx}}{2}\right)}\cdot\frac{\sin\left(\frac{n_y\overline{\psi}_{HPx}}{2}\right)}{n_y\sin\left(\frac{\overline{\psi}_{HPx}}{2}\right)}\right|^m = \frac{1}{\sqrt{2}} \tag{2.29}$$

$$\left|\frac{\sin\left(\frac{n_x\overline{\psi}_{HPy}}{2}\right)}{n_x\sin\left(\frac{\overline{\psi}_{HPy}}{2}\right)}\cdot\frac{\sin\left(\frac{n_y\psi_{HPy}}{2}\right)}{n_y\sin\left(\frac{\psi_{HPy}}{2}\right)}\right|^m = \frac{1}{\sqrt{2}} \tag{2.30}$$

In (2.29) ψ_{HPx} and $\overline{\psi}_{HPx}$ define a half-power point on the *x*-*r* plane. The two polar angles describing this point, A, are measured from the *x*- and *y*-axes and are labeled as $\theta_x^{HP_x}$ and $\theta_y^{HP_x}$ in Figure 2.3. Similarly, ψ_{HPy} and $\overline{\psi}_{HPy}$ in (2.30) describe a half-power point in the *y*-*r* plane and the polar illustration of this point are $\theta_x^{HP_y}$ and $\theta_y^{HP_y}$. Assuming that the four half power points i.e. two in the *x*-*r* plane and two in the *y*-*r* plane, are in the visible range, a case of practical interest for most situations, ψ_{HPx} and ψ_{HPy} with the help of (2.28) can be determined with the following results.

$$\psi_{HPx} = \beta d_x \tan\left(\frac{HPBW_x}{2}\right)\sqrt{\cos^2\left(\frac{HPBW_x}{2}\right) - \cos^2\theta_{0x}} \tag{2.31}$$

$$\psi_{HPy} = \beta d_y \tan\left(\frac{HPBW_y}{2}\right)\sqrt{\cos^2\left(\frac{HPBW_y}{2}\right) - \cos^2\theta_{0y}} \tag{2.32}$$

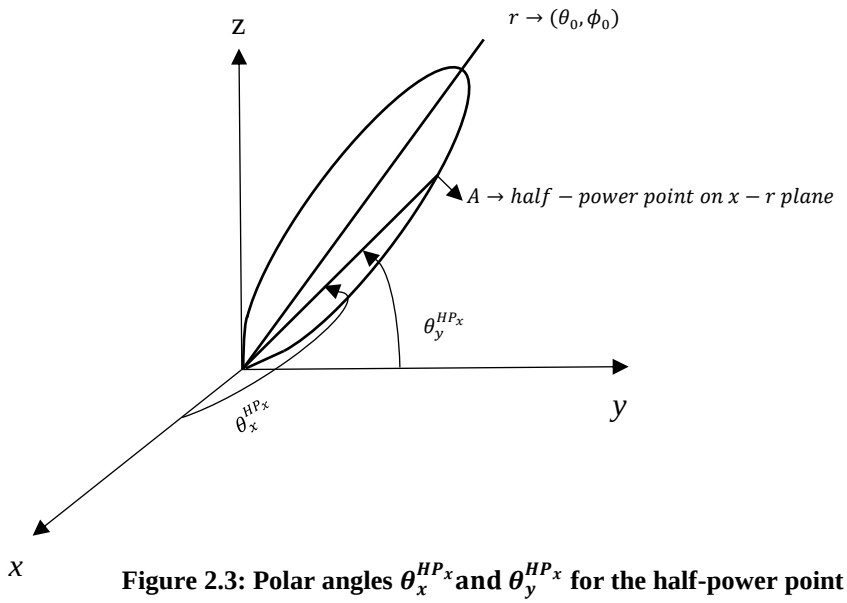

Figure 2.3: Polar angles $\theta_x^{HP_x}$ and $\theta_y^{HP_x}$ for the half-power point A on *x-r* plane

Furthermore, for the half power points associated with $HPBW_x$, the value of ψ_y is denoted as $\overline{\psi}_{HP_x}$ and can be calculated using (2.33). Similarly, for the half power points associated with the $HPBW_y$, the value of ψ_x is denoted as $\overline{\psi}_{HP_y}$ and is obtained from (2.34)

$$\overline{\psi}_{HPx} = \psi_y\big|_{\theta_y=\theta_y^{HPx}} = \left(\frac{2\pi d_y}{\lambda}\right)(\cos\theta_y^{HPx} - \cos\theta_{0y}) \tag{2.33}$$

$$\overline{\psi}_{HPy} = \psi_x\big|_{\theta_x=\theta_x^{HPy}} = \left(\frac{2\pi d_x}{\lambda}\right)(\cos\theta_x^{HPy} - \cos\theta_{0x}) \tag{2.34}$$

The angles θ_y^{HPx} in (2.33) and θ_x^{HPy} in (2.34) need further examination. In doing so, first Figure 2.4 depicting the *x-r* plane in which a vector $\overrightarrow{OA}$ extending from the origin to the half power point A is considered. The angle between the vector $\overrightarrow{OA}$ and the *x*-axis is denoted as $\theta_x^{HP_x}$. The vector $\overrightarrow{OB}$ is in the direction of the boresight and at the same height as $\overrightarrow{OA}$. The angle between $\overrightarrow{OB}$ and $\overrightarrow{OA}$ is denoted as α. To obtain a relationship for θ_y^{HPx}, we proceed as follows.

$$\cos\theta_y^{HPx} = \widehat{a_y} \cdot \frac{\overrightarrow{OA}}{|\overrightarrow{OA}|}$$

$$\theta_{0x} = \alpha + \theta_x^{HPx}$$

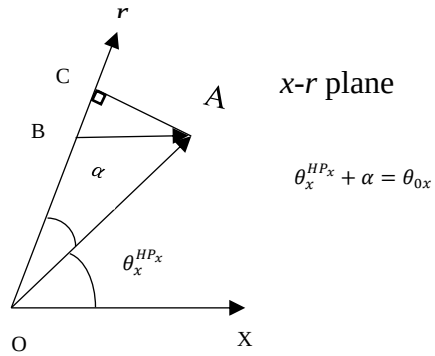

Figure 2.4: *x-r* plane depicting $\boldsymbol{\theta_x^{HP_x}}$, $\boldsymbol{\alpha}$, $\overrightarrow{\boldsymbol{OA}}$, $\overrightarrow{\boldsymbol{OB}}$ and $\overrightarrow{\boldsymbol{BA}}$

$$\overrightarrow{OA} = \overrightarrow{OB} + \overrightarrow{BA}$$

$$\overrightarrow{OB} = \left|\overrightarrow{OB}\right| \widehat{a_r}\ ,\ \overrightarrow{BA} = \left|\overrightarrow{BA}\right| \widehat{a_x}$$

where $\widehat{a_r}$ is the unit vector along the radial line representing the boresight direction in the *x-r* plane, $\widehat{a_x}$ is the unit vector along the *x*-axis and $\widehat{a_y}$ is the unit vector along the *y*-axis. Then the dot product of $\widehat{a_y}$ and $\overrightarrow{OA}$ yields

$$\widehat{a_y} \cdot \overrightarrow{OA} = \widehat{a_y} \cdot \left(\left|\overrightarrow{OB}\right|\widehat{a_r} + \left|\overrightarrow{BA}\right|\widehat{a_x}\right)$$

$$= \left|\overrightarrow{OB}\right|\widehat{a_y} \cdot \widehat{a_r} + \left|\overrightarrow{BA}\right|\widehat{a_y} \cdot \widehat{a_x}$$

$$= \left|\overrightarrow{OB}\right| \cos\theta_{0y}$$

$$\cos\theta_y^{HPx} = \frac{\left|\overrightarrow{OB}\right|}{\left|\overrightarrow{OA}\right|} \cos\theta_{0y} = \frac{OB}{OA}\cos\theta_{0y}$$

$$OB = OC - BC = OA\cos\alpha - BC$$

$$= OA\cos\alpha - \frac{AC}{\tan(\alpha + \theta_x^{HPx})}$$

Note that $$A\hat{B}C = \alpha + \theta_x^{HPx}$$

$$\tan(\alpha + \theta_x^{HPx}) = \frac{AC}{BC} \text{ and } \alpha + \theta_x^{HPx} = \theta_{0x}$$

But, $AC = OA\sin\alpha \rightarrow OB = \left[\cos\alpha - \frac{\sin\alpha}{\tan(\theta_{0x})}\right]\cos\theta_{oy}$

$$\cos\theta_y^{HPx} = \frac{\cos\theta_{0y}}{\sin\theta_{0x}}\,(\sin\theta_{0x}\cos\alpha - \cos\theta_{0x}\sin\alpha\,)$$

$$= \frac{\cos\theta_{0y}}{\sin\theta_{0x}}\sin(\theta_{0x}-\alpha) = \frac{\cos\theta_{0y}}{\sin\theta_{0x}}\sin(\theta_x^{HPx})$$

Now,

$$\overline{\psi}_{HPx} = \left(\frac{2\pi d_y}{\lambda}\right)\left(\frac{\cos\theta_{0y}}{\sin\theta_{0x}}\sin(\theta_x^{HPx}) - \cos\theta_{0y}\right) = \; -\left(\frac{2\pi d_y}{\lambda}\right)\cos\theta_{0y}\left(1 - \frac{\sin\theta_x^{HPx}}{\sin\theta_{0x}}\right)$$

On the other hand,

$$\psi_{HPx} = \left(\frac{2\pi d_x}{\lambda}\right)(\cos\theta_x^{HPx} - \cos\theta_{0x})$$

$$\cos\theta_x^{HPx} \;= \left(\frac{\lambda}{2\pi d_x}\right)\psi_{HPx} + \cos\theta_{0x}$$

$$= \left(\frac{\lambda}{2\pi d_x}\right)\left(\frac{2\pi d_x}{\lambda}\right)\tan\left(\frac{HPBW_x}{2}\right)\sqrt{\cos^2\left(\frac{HPBW_x}{2}\right) - \cos^2\theta_{0x}} + \;\cos\theta_{0x}$$

$$= \tan\left(\frac{HPBW_x}{2}\right)\sqrt{\cos^2\left(\frac{HPBW_x}{2}\right) - \cos^2\theta_{0x}} + \;\cos\theta_{0x}$$

$$\sin\theta_x^{HPx} = \sqrt{1-\cos^2\theta_x^{HPx}}$$

$$= \left\{1 - \tan^2\left(\frac{HPBW_x}{2}\right)\left[\cos^2\left(\frac{HPBW_x}{2}\right) - \cos^2\theta_{0x}\right] - \cos^2\theta_{0x} - 2\cos\theta_{0x}\tan\left(\frac{HPBW_x}{2}\right)\sqrt{\cos^2\left(\frac{HPBW_x}{2}\right) - \cos^2\theta_{0x}}\;\right\}^{\frac{1}{2}}$$

$$= \left\{1 - \sin^2\left(\frac{HPBW_x}{2}\right) + \tan^2\left(\frac{HPBW_x}{2}\right)\cos^2\theta_{0x} - \cos^2\theta_{0x} - 2\cos\theta_{0x}\tan\left(\frac{HPBW_x}{2}\right)\sqrt{\cos^2\left(\frac{HPBW_x}{2}\right) - \cos^2\theta_{0x}}\;\right\}^{\frac{1}{2}}$$

$$= \left\{\left[\cos^2\left(\frac{HPBW_x}{2}\right) - \cos^2\theta_{0x}\right] + \left[\tan\left(\frac{HPBW_x}{2}\right)\cos\theta_{0x}\right]^2 - 2\cos\theta_{0x}\tan\left(\frac{HPBW_x}{2}\right)\sqrt{\cos^2\left(\frac{HPBW_x}{2}\right) - \cos^2\theta_{0x}}\right\}^{\frac{1}{2}}$$

$$= \left\{\left[\tan\left(\frac{HPBW_x}{2}\right)\cos\theta_{0x} - \sqrt{\cos^2\left(\frac{HPBW_x}{2}\right) - \cos^2\theta_{0x}}\right]^2\right\}^{\frac{1}{2}}$$

$$= \left|\tan\left(\frac{HPBW_x}{2}\right)\cos\theta_{0x} - \sqrt{\cos^2\left(\frac{HP_{BWEx}}{2}\right) - \cos^2\theta_{0x}}\right|$$

Hence,

$$\overline{\psi}_{HPx} = -\left(\frac{2\pi d_y}{\lambda}\right)\cos\theta_{0y}\left[1 - \frac{\left|\tan\left(\frac{HPBW_x}{2}\right)\cos\theta_{0x} - \sqrt{\cos^2\left(\frac{HPBW_x}{2}\right) - \cos^2\theta_{0x}}\right|}{\sin\theta_{0x}}\right]$$

$$= -\left(\frac{2\pi d_y}{\lambda}\right)\cos\theta_{0y}\left[1 - \left|\tan\left(\frac{HPBW_x}{2}\right)\cot\theta_{0x} - \frac{\sqrt{\cos^2\left(\frac{HPBW_x}{2}\right) - \cos^2\theta_{0x}}}{\sin^2\theta_{0x}}\right|\right]$$

$$= -\left(\frac{2\pi d_y}{\lambda}\right)\cos\theta_{0y}\left[1 - \left|\tan\left(\frac{HPBW_x}{2}\right)\cot\theta_{0x} - \sqrt{\cos^2\left(\frac{HPBW_x}{2}\right)(1+\cot^2\theta_{0x}) - \cot^2\theta_{0x}}\right|\right]$$

$$= -\left(\frac{2\pi d_y}{\lambda}\right)\cos\theta_{0y}\left[1 - \left|\tan\left(\frac{HPBW_x}{2}\right)\cot\theta_{0x} - \sqrt{\cos^2\left(\frac{HPBW_x}{2}\right) - \cot^2\theta_{0x}\left(1 - \underbrace{\cos^2\left(\frac{HPBW_x}{2}\right)}_{\sin^2\left(\frac{HP_x}{2}\right)}\right)}\right|\right]$$

$$= -\left(\frac{2\pi d_y}{\lambda}\right)\cos\theta_{0y}\left[1 - \left|\tan\left(\frac{HPBW_x}{2}\right)\cot\theta_{0x} - \cos\left(\frac{HPBW_x}{2}\right)\sqrt{1 - \tan^2\left(\frac{HPBW_x}{2}\right)\cot^2\theta_{0x}}\right|\right]$$

Let $Q_x = \tan\left(\frac{HPBW_x}{2}\right)\cot\theta_{0x}$

Then,

$$\overline{\psi}_{HPx} = -\left(\frac{2\pi d_y}{\lambda}\right)\cos\theta_{0y}\left[1-\left|Q_x-\cos\left(\frac{HPBW_x}{2}\right)\sqrt{1-Q_x^2}\right|\right] \qquad (2.35)$$

Similarly, it can be shown that

$$\overline{\psi}_{HPy} = -\left(\frac{2\pi d_x}{\lambda}\right)\cos\theta_{0x}\left[1-\left|Q_y-\cos\left(\frac{HPBW_y}{2}\right)\sqrt{1-Q_y^2}\right|\right] \qquad (2.36)$$

where $Q_y = \tan\left(\frac{HPBW_y}{2}\right)\cot\theta_{0y}$.

Equations (2.29) to (2.36) can be used in an analysis process where the array factor is known and half-power beamwidths in the *x-r* and *y-r* planes are calculated. The same equations are also used in a synthesis process where the beamwidths and side lobe level are known and array parameters $n_x, n_y,$ and m together with element currents are determined.

2.5 Element Excitation Currents

2.5.1 Revisiting Calculation of Currents for NUELA

It was shown in [24] that for a linear array with even or odd number of elements, the radiation pattern of NUELA for given design parameters n and m, can be treated as a power series with finite number of terms. For *N* number of elements, the array factor can be written as a polynomial of order $N-1$ as given in (2.37)

$$AF = \left(\frac{\sin\left(\frac{n\psi}{2}\right)}{n\sin\left(\frac{\psi}{2}\right)}\right)^m = \left(\sum_{k=0}^{n-1} Z^k\right)^m = \sum_{p=0}^{N-1} I_p Z^p \qquad (2.37)$$

where $Z = e^{j\psi}$ in which $\psi = \left(\frac{2\pi d}{\lambda}\right)(cos\theta - cos\theta_0)$, N can be calculated according to (2.37) if the design parameters n and m are known. The parameter n is the number of elements in an equivalent building block uniformly excited array and m is a positive real number.

$$N = (n-1)m + 1 \qquad (2.38)$$

The excitation coefficient of each element in NUELA, denoted by I_p in (2.37), was calculated by treating it as a coefficient of a finite power series. A recursive relationship was developed in [24] for the excitation of the pth element such that the end element currents were normalized to unity, i.e. $I_0 = 1$. This relationship is given as

$$I_p = \frac{1}{p}\sum_{i=1}^{p}(im - p + i)I_{p-i}\, for\ 1 \le p \le N_c$$

$$I_p = I_{N-p-1}\, for\ N_c \le p \le N-1$$

and N_c depicts the center element(s) which is given by $N_c = \begin{cases} \frac{N-2}{2}, & for\ N\ even \\ \frac{N-1}{2}, & for\ N\ odd. \end{cases}$ (2.39)

It must be noted that the method of computing the excitation coefficients used in (2.39) is only valid for symmetric arrays. When such is the case, $Z = e^{j\psi}$ can be expanded using Euler's formula and the array factor in (2.37) can be reconstructed using the excitation coefficients calculated in (2.39) as follows

$$AF\ (\theta, \phi) = 2\sum_{i=0}^{N_c} I_{N_c-i}\cos\left[\left(\frac{2i+1}{2}\right)\left(\frac{2\pi d}{\lambda}\right)(\cos\theta - \cos\theta_0)\right]\ for\ N\ even \tag{2.40}$$

$$AF\ (\theta, \phi) = I_{N_c} + 2\sum_{i=1}^{N_{cx}} I_{N_c-i}\cos\left[i\ \frac{2\pi d}{\lambda}\ (\cos\theta - \cos\theta_0)\right]\ for\ N\ odd \tag{2.41}$$

2.5.2 Calculation of Currents for Low Side Lobe Nonuniformly Excited Planar Arrays

The results obtained above are extended in this section to compute the total number of elements of the proposed array and the associated array excitation coefficients. For a known n_x, n_y and m, the total number of elements for the proposed planar arrays are determined by first calculating the total number of elements along the *x*- and *y*-axes in each constituent NUELA.

$$N = N_x \cdot N_y = [(n_x - 1)m + 1][(n_y - 1)m + 1] \tag{2.42}$$

The array factor in terms of element currents is obtained by re-writing the constituent array factors in (2.6) in the form of (2.37). This is done as follows

$$|AF(\theta,\phi)| = |AF_x(\theta,\phi)| \cdot |AF_y(\theta,\phi)|$$

$$= \left| \sum_{p=0}^{N_x-1} I_p Z_x^p \sum_{q=0}^{N_y-1} I_q Z_y^q \right| = \sum_{p=0}^{N_x-1} \sum_{q=0}^{N_y-1} I_{pq}\, Z_x^p Z_y^q \tag{2.43}$$

where $Z_x = e^{j\psi_x}$ and $Z_y = e^{j\psi_y}$. Since the above procedure is based on separable distribution, it can be stated that the excitation coefficient of a planar array element that lies on the *xy* plane and is indexed as the pq^{th} element can be expressed as $I_{pq} = I_p I_q$ where I_p and I_q are the excitation coefficients of pth and q^{th} elements in a NUELA placed along the *x*- and *y*-axes respectively. The excitation coefficient of each constituent linear array is computed in a similar manner as (2.39) and I_{pq} can then be expressed as

$$I_{pq} = I_p I_q$$

$$= \left[\frac{1}{p} \sum_{i=1}^{p} (im - p + i) I_{p-i}\right] \left[\frac{1}{q} \sum_{i=1}^{q} (im - q + i) I_{q-i}\right] \tag{2.44}$$

By extending the observation made in (2.39) it can be further said that $I_0 = 1$, $1 \le p \le N_{cx}$ and that $I_p = I_{N_x-p-1}$ for $N_{cx} \le p \le N_x - 1$. Similarly, $1 \le q \le N_{cy}$ and $I_q = I_{N_y-q-1}$ for $N_{cy} \le q \le N_y - 1$. The center elements N_{cx} and N_{cy} can then be expressed as

$$N_{cx} = \begin{cases} \frac{N_x-2}{2}, & for\ N_x\ even \\ \frac{N_x-1}{2}, & for\ N_x\ odd \end{cases} \quad \text{and} \quad N_{cy} = \begin{cases} \frac{N_y-2}{2}, & for\ N_y\ even \\ \frac{N_y-1}{2}, & for\ N_y\ odd \end{cases} \tag{2.45}$$

The $Z_x = e^{j\psi_x}$ and $Z_y = e^{j\psi_y}$ in (2.43) can be expanded in a similar manner as discussed in the section above and each NUELA component being a symmetric array with respect to the center element can have different analytical expressions for different geometries depending upon whether $N = N_x$ or N_y are either even or odd. Using (2.40) and (2.41), the array factor for even and odd N can be expressed as given in(2.46) and (2.47), respectively.

For N_x even:

$$AF_x\,(\theta,\phi) = 2 \sum_{i=0}^{N_{cx}} I_{N_{cx}-i} \cos\left[\frac{2i+1}{2}\,\frac{2\pi d_x}{\lambda}\,(\sin\theta\cos\phi - \sin\theta_0\cos\phi_0)\right] \tag{2.46a}$$

For N_y even:

$$AF_y\ (\theta, \phi) = 2 \sum_{i=0}^{N_{cy}} I_{N_{cy}-i} \cos\left[\frac{2i+1}{2}\ \frac{2\pi d_y}{\lambda}\ (\sin\theta \sin\phi - \sin\theta_0 \sin\phi_0)\right] \quad (2.46b)$$

For N_x odd:

$$AF_x\ (\theta, \phi) = I_{N_{cx}} + 2 \sum_{i=1}^{N_{cx}} I_{N_{cx}-i} \cos\left[i\ \frac{2\pi d_x}{\lambda}\ (\sin\theta \cos\phi - \sin\theta_0 \cos\phi_0)\right] \quad (2.47a)$$

For N_y odd:

$$AF_y\ (\theta, \phi) = I_{N_{cy}} + 2 \sum_{i=1}^{N_{cy}} I_{N_{cy}-i} \cos\left[i\ \frac{2\pi d_y}{\lambda}\ (\sin\theta \sin\phi - \sin\theta_0 \sin\phi_0)\right] \quad (2.47b)$$

Chapter 3: Radiation Characteristics of Low Side Lobe Planar Arrays

The performance of the proposed low side lobe non-uniformly excited planar array is assessed by calculating the directivity (D), HPBW, SLL, and the excitation current amplitudes. Using these quantities, we can determine radiation intensity directed towards a desired direction, energy propagation in unwanted directions, and the necessary information needed to design the feed network. The information on the array radiation characteristics is also required in designing communication links. The analytical results derived in Chapter 2 are used in this chapter to study variations in D, HPBW, SLL and the excitation current amplitudes with respect to array parameters n_x, n_y, m, θ_0 and ϕ_0. Simulations results are generated for $0 \leq \theta_0 \leq 60°$. It is pertinent to note that most applications of arrays require scanning in that range. Moreover, ϕ_0 is set to be between $0 \leq \phi_0 \leq 90°$ as any range extending beyond 90° would simply repeat the results derived within this range due to the array symmetric current distribution. As discussed in the previous chapter, altering n_x, n_y or m would vary the total number of elements in the array which in turn would influence HPBW, SLL and D. These variations are tabulated, simulated and discussed in the following sections.

3.1 Directivity

The directivity of any radiating system is defined as the ratio of the radiation intensity in the direction of maximum radiation to the radiation intensity averaged over all directions [27], where the radiation intensity is the power radiated by the antenna in a unit solid angle. (4π stradians for the entire space). The directivity of the proposed planar array is computed here and its variations with the array parameters are assessed. In general, the directivity of an antenna can be calculated using the expression below

$$D = \frac{4\pi}{\int_{\theta=0}^{\pi} \int_{\varphi=0}^{2\pi} |F(\theta,\varphi|^2 \sin\theta d\theta d\varphi} \tag{3.1}$$

where $|F(\theta, \phi)|$ is the normalized pattern. The directivity in dB is then calculated using

$$D\ (dB) = 10log_{10}(D) \tag{3.2}$$

Numerical results for directivity are obtained for low side lobe planar arrays with parameters $4 \leq n_x \leq 5, 5 \leq n_y \leq 9$ and $1 \leq m < 4$ and various boresight directions defined by θ_0 and ϕ_0. Tables 3.1 to 3.4 summarize these results. In these tables, the column with $m = 1$ represents the directivity of a uniformly excited planar array, in which case n_x and n_y represent the actual number of array elements along the *x*- and *y*-axes. It is observed that in all tables, the directivity of the planar array increases when the parameter m increases. The increase of directivity gradually reduces as m is increased further. It is also observed that the proposed array gives the best directivity performance when the pattern maximum is in the broadside direction, i.e. $\theta_0 = 0°$ or $\theta_{0x} = \theta_{0y} = 90°$ in Table 3.1. Any directivity for given values of n_x, n_y and m in Table 3.1 is larger than the corresponding one in Tables 3.2 to 3.4. In other words, the directivity of the array reduces as the main lobe is steered away from the normal to the plane of array.

Irrespective of the array main beam direction, it can be stated that the directivity increases when the array size is increased, but the increase is more significant when the number of elements of the array is expanded by increasing m than by increasing either n_x or n_y. Directivity values in Tables 3.1 to 3.4 also reveal that as the difference between parameters n_x and n_y increases, the array becomes more directive. In other words, the more rectangular an array, the better its directivity. Also, comparison of directivity values in Table 3.2 with those in Table 3.3 and Table 3.4 indicates that the directivity is influenced more strongly by steering the main beam in the elevation (θ_0) than in the azimuthal (ϕ_0) direction.

Some important trends observed above are further analyzed by plotting directivity as a function of $\theta_0, \phi_0, n_x, n_y$ or m parameter. Figures 3.1 to 3.3 illustrate these variations where in each plot, the relationship between the directivity and the above mentioned parameters is depicted by varying only one parameter while keeping all the others constant. These results are further discussed below.

Figure 3.1 shows variations of directivity with θ_0 for several values of m, while n_x, n_y and ϕ_0 are kept constant and with element spacings $d_x = d_y = \lambda/2$. This figure confirms a behavior observed earlier when examining results in Tables 3.1-3.4 that as the main beam is steered away from the z-axis ($\theta_0 = 0°$) the directivity decreases. Also, it appears that the decrease in directivity with increasing elevation angle is nearly independent of parameter *m*.

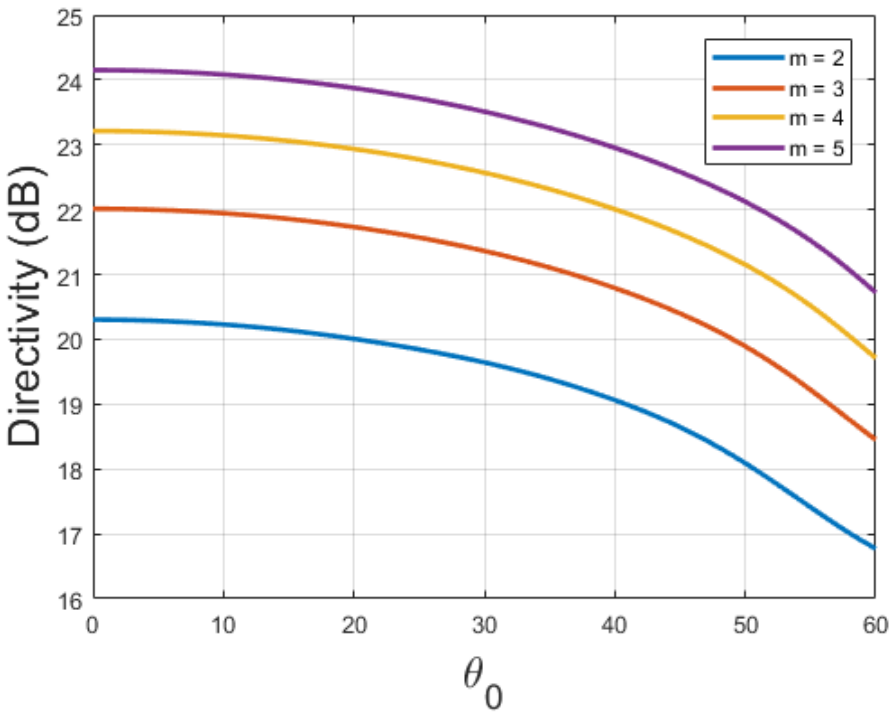

Figure 3.1: Variations of D (dB) versus θ_0(deg) for $\phi_0 = 25°, n_x 8, n_y = 4, 2 \leq m \leq 5$ and $d_x = d_y = \lambda/2$

Figure 3.2 examines variations of directivity versus the azimuthal angle ϕ_0. It is noted that rotating the main lobe along ϕ direction by varying ϕ_0, while keeping θ_0, m, n_x and n_y constant, has negligible impact on directivity. Therefore, it can be stated that generally when the main lobe is scanned in the azimuthal direction, the directivity performance is not affected significantly. This behavior may be attributed to the fact that varying ϕ_0 does not result in appreciable beam broadening. As expected, larger values of *m* correspond to higher directivities, but it is clearly noted that directivity increases more slowly for larger values of *m*, confirming the same observation made when examining the data in Tables 3.1 to 3.4.

Table 3.1 Directivity in dB for planar arrays with $d_x = d_y = \lambda/2$, θ_0= 0°, ϕ_0= 0°, and several values of n_x , n_y, and m

n_x, n_y/m	1	2	3	4
4,5	14.395	18.179	19.91	21.113
4,6	15.332	19.017	20.733	21.934
4,7	15.962	19.706	21.421	22.621
4,8	16.618	20.303	22.012	23.212
4,9	17.11	20.823	22.532	23.732
5,5	15.278	19.205	20.937	22.137
5,6	16.211	20.043	21.759	22.959
5,7	16.823	20.731	22.447	23.646
5,8	17.488	21.328	23.039	24.237
5,9	17.962	21.848	23.558	24.756

Table 3.2 Directivity in dB for planar arrays with $d_x = d_y = \lambda/2$, θ_0 = 30°, ϕ_0=25°, and several values of n_x, n_y, and m

n_x, n_y/m	1	2	3	4
4,5	13.943	17.702	19.45	20.661
4,6	14.813	18.539	20.275	21.484
4,7	15.475	19.231	20.964	22.172
4,8	16.086	19.827	21.557	22.764
4,9	16.613	20.35	22.077	23.284
5,5	14.895	18.745	20.487	21.693
5,6	15.779	19.582	21.312	22.516
5,7	16.426	20.273	22.000	23.204
5,8	17.039	20.869	22.593	23.796
5,9	17.565	21.391	23.113	24.316

Table 3.3 Directivity in dB for planar arrays with $d_x = d_y = \lambda/2$, θ_0 =30°, ϕ_0= 40°,and several values of n_x, n_y, and m

n_x, n_y/m	1	2	3	4
4,5	13.8	17.482	19.235	20.451
4,6	14.593	18.317	20.063	21.276
4,7	15.323	19.017	20.754	21.966
4,8	15.914	19.614	21.348	22.558
4,9	16.426	20.137	21.869	23.079
5,5	14.83	18.54	20.276	21.485
5,6	15.607	19.374	21.104	22.311
5,7	16.352	20.075	21.795	23.000
5,8	16.94	20.672	22.388	23.593
5,9	17.445	21.194	22.909	24.113

Table 3.4 Directivity in dB for planar arrays with $d_x = d_y = \lambda/2$, θ_0 =60°,ϕ_0= 25°, and several values of n_x, n_y,and m

n_x, n_y/m	1	2	3	4
4,5	12.114	14.972	16.5	17.61
4,6	12.871	15.775	17.311	18.428
4,7	13.514	16.452	17.994	19.114
4,8	14.074	17.037	18.583	19.706
4,9	14.574	17.553	19.101	20.225
5,5	12.979	15.831	17.391	18.564
5,6	13.752	16.636	18.209	19.394
5,7	14.394	17.315	18.898	20.089
5,8	14.951	17.902	19.491	20.686
5,9	15.451	18.418	20.012	21.21

As a last case of directivity performance evaluation, variations of D versus θ_0 for several values of n_x are presented in Figure 3.3. The trends in this figure are similar to those in Figure 3.1 discussed above. However, comparison of these two figures indicates that directivity increases more slowly with n_x than with m. In summary, the results presented in Tables 3.1 to 3.4 and Figures 3.1 to 3.3 capture the underlying trends in dependence of directivity on the planar array parameters.

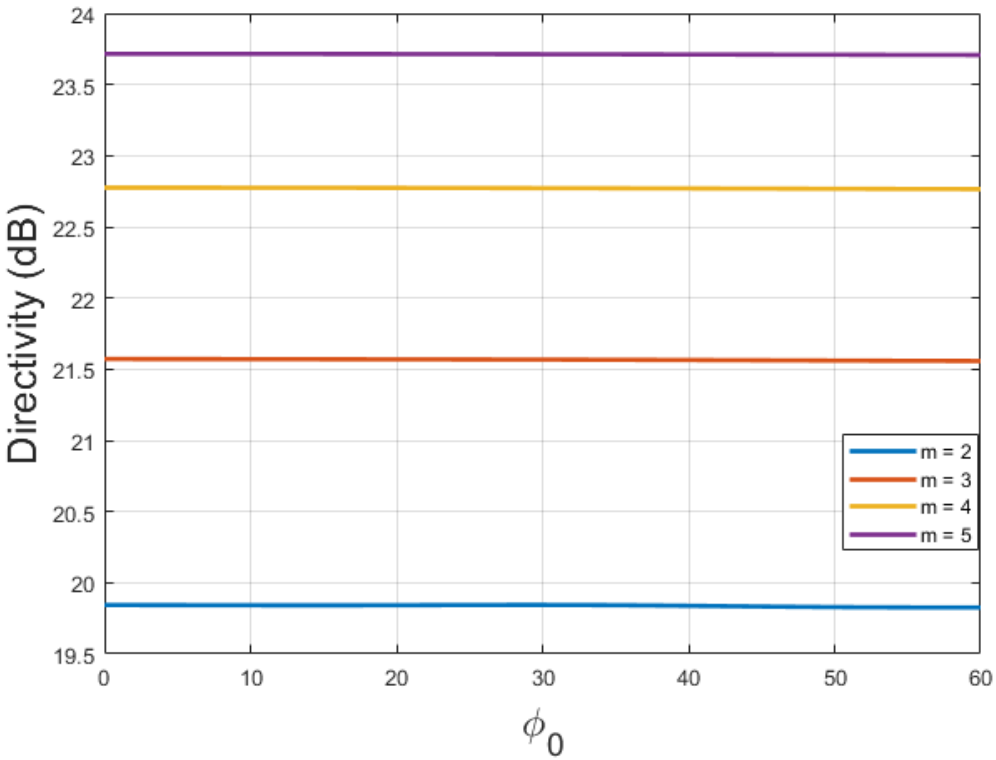

Figure 3.2: Variations of D (dB) versus ϕ_0(deg) for $\theta_0 = 25°, n_x = 8, n_y = 4, 2 \leq m \leq 5$ and $d_x = d_y = \lambda/2$

3.2 Side Lobe Level

Although highly directive antenna arrays have the ability to direct most of the power in a desired direction, it is essential to maintain a sufficiently low side lobe level to ensure that propagation in unwanted directions does not adversely affect the operation of other systems. Therefore, calculation of SLL for low side lobe planar arrays is an important task undertaken in this section. As discussed in section 2.3.1, SLL can be determined by

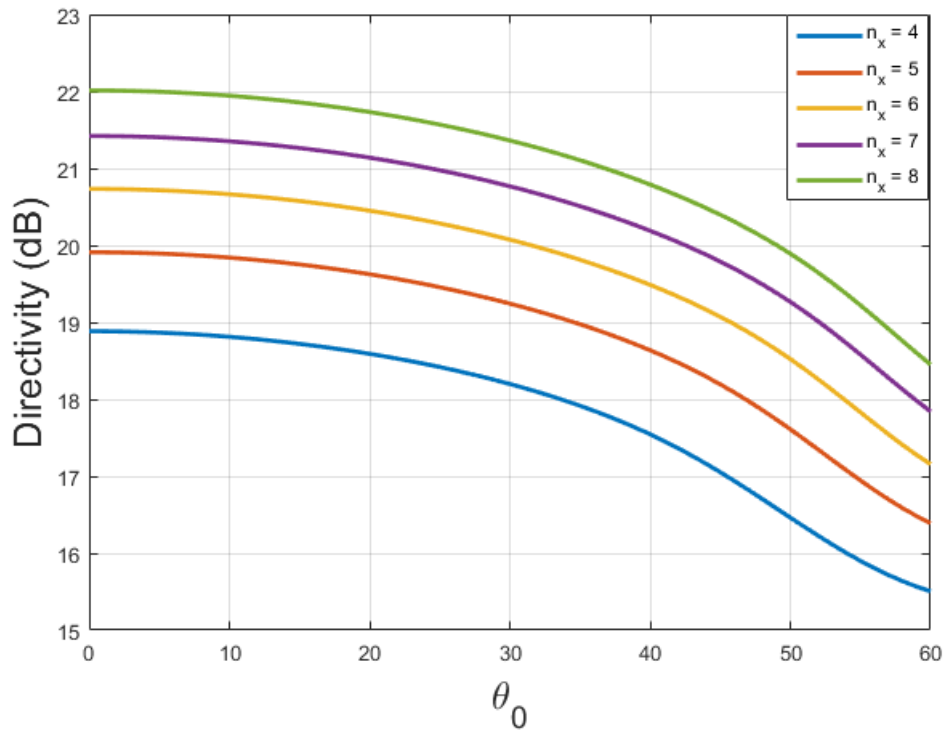

Figure 3.3: Variations of D (dB) versus θ_0(deg) for $\phi_0 = 25°$, $m = 3, n_y = 4 \leq n_x \leq 8$, and $d_x = d_y = \lambda/2$

finding the second highest peak value of the array factor plot in the θ, ϕ domain. In general, a systematic approach for determining the SLL value of a two-dimensional array such as the proposed planar array is to find all points at which $\frac{\partial AF(\theta,\phi)}{\partial \theta} = 0$ and $\frac{\partial AF(\theta,\phi)}{\partial \phi} = 0$, then all the maxima points are sorted and the second largest value is selected. This method of calculation of SLL can be implemented numerically.

For the proposed array, an analytical method for the calculation of SLL, as discussed in section 2.3.2, can be used. In doing so, applicable conditions (2.16) and (2.17) are first determined and accordingly, the SLL point is calculated using (2.14) or (2.15). The SLL point is then substituted in (2.10) to determine the SLL. In this section, the SLL of the proposed array is determined using the above steps for the case when $n_x < n_y$ and $n_x \geq 3$. It is emphasized that the SLL calculated using the analytical method described above is valid if the condition (2.22) or (2.23) is satisfied. Furthermore, it is assumed that no grating lobe contributes to SLL. When the required conditions are satisfied, the SLL of a rectangular planar array is determined by the number of elements placed along its shorter

side. Therefore, even if more elements are placed along the longer side of the array SLL remains the same, while the directivity increases. This is an interesting case of increasing the directivity without any degradation in SLL.

Side lobe levels for planar arrays with different sets of parameters are calculated. The results are presented in Table 3.5. In this table n_s is the smaller of n_x and n_y. Examination of results in Table 3.5 reveals that SLL decreases across the rows and columns, that is when both n_s and m increase. However, the decrease in SLL due to m is more dominant over the decrease due to n_s.

Figure 3.4 depicts variations of SLL versus n_s for several values of m. It is observed that SLL of the proposed array reduces as the number of elements along the smaller side of the rectangular array (n_s) is increased. It is also noted that SLL for any given m and n_s reaches a saturation point.

Table 3.5: SLL in dB for planar array with $d_x = d_y = \lambda/2$, θ_0 = 0°, and several values of m and n_s (smaller of n_x and n_y)

n_s/m	2	3	4	5
3	−19.085	-28.627	-38.17	-47.712
4	22.607	-33.91	-45.213	-56.517
5	-24.083	-36.124	-48.165	-60.206
6	-24.851	-37.277	-49.703	-62.129
7	-25.305	-37.958	-50.61	-63.263
8	-25.596	-38.393	-51.191	-63.989
9	-25.793	-38.689	-51.586	-64.482
10	-25.933	-38.9	-51.867	-64.834
11	-26.037	-39.055	-52.074	-65.092
12	-26.115	-39.173	-52.231	-65.288

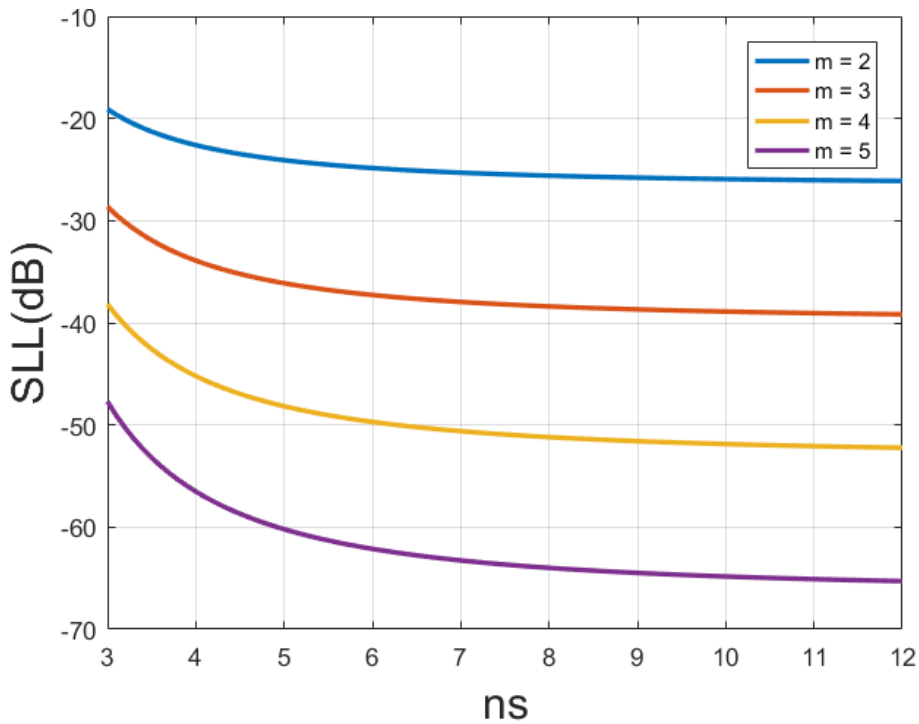

Figure 3.4: Variations of SLL versus n_s for $2 \leq m \leq 5$ and $d_x = d_y = \lambda/2$

after a certain values of n_s. This phenomenon is inherent in uniformly excited arrays which are building blocks for the low side lobe planar arrays introduced here.

3.3 Half-Power Beamwidth

The half-power beam width (HPBW) describes the angular separation between two points on the main lobe that have a radiation intensity equal to half of that for the maximum radiation point. The two points lie on the main lobe and share the same plane as the maximum radiation intensity point.

The HPBW of the array was analytically defined using the *x-r* and *y-r* planes in section 2.4.2. In order to calculate $HPBW_x$, (2.31) and (2.35) are substituted in (2.29), and for $HPBW_y$, (2.32) along with (2.36) are substituted in (2.30). The resulting expressions relate $HPBW_x$ and $HPBW_y$ to n_x, n_y and m. Since θ_{0y} and θ_{0x} are both functions of θ_0 and ϕ_0, it can said that the above HPBW expressions are functions of parameters $\theta_0, \phi_0, n_x, n_y$ and m, which can be solved for $HPBW_x$ and $HPBW_y$ using MATLAB for

any known set of parameters. Numerical results for $HPBW_x$ and $HPBW_y$ for a number of example cases are calculated and presented in Tables 3.6 to 3.9.

Tables 3.6 and 3.7 show half-power beamwidth results for a broadside case, i.e. $\theta_0 = 0°$ or equivalently $\theta_{0x} = \theta_{0y} = 90°$. For such a case, $\sin\left(\frac{n_y\bar{\psi}_{HPx}}{2}\right)/n_y \sin\left(\frac{\bar{\psi}_{HPx}}{2}\right) = \sin\left(\frac{n_x\bar{\psi}_{HPy}}{2}\right)/n_x \sin\left(\frac{\bar{\psi}_{HPy}}{2}\right) = 1$ in (2.29) and (2.30), and the $HPBW_x$ and $HPBW_y$ can be determined by ψ_{HP_x} and ψ_{HP_y} alone. Examination of results in Table 3.6 indicates that $HPBW_x$ changes with n_x whereas $HPBW_y$ does not vary with n_x. Similarly, in Table 3.7, only $HPBW_y$ changes with n_y. For a constant value of the exponent m in Table 3.6, as the value of n_x increases, $HPBW_x$ reduces while $HPBW_y$ remains constant. Similarly in Table 3.7, $HPBW_y$ reduces when n_y is increased and $HPBW_x$ remains unchanged. Comparison of Tables 3.6 and 3.7 shows that for a broadside case, $HPBW_x$ for $\{n_x = 5, n_y = 4\}$ is the same as $HPBW_y$ for $\{n_x = 4, n_y = 5\}$. Therefore, when the rectangular array is rotated by 90°about its center, the HPBW in the *x*-*r* plane of the old pattern becomes the HPBW in *y*-*r* plane of the new pattern and vice versa. In summary, both $HPBW_x$ and $HPBW_y$ are reduced when the value of exponent *m* is increased for any given n_x and n_y.

Tables 3.8 and 3.9 present beamwidth results for a case when the main beam is steered away from the z-axis ($\theta_0 \neq 0°$).Therefore, $\sin\left(\frac{n_y\bar{\psi}_{HPx}}{2}\right)/n_y \sin\left(\frac{\bar{\psi}_{HPx}}{2}\right) \neq 1$, $\sin\left(\frac{n_x\bar{\psi}_{HPy}}{2}\right)/n_x \sin\left(\frac{\bar{\psi}_{HPy}}{2}\right) \neq 1$, and $HPBW_x$ as well as $HPBW_y$ depend on both n_x and n_y. However, calculated HPBW values in Table 3.8 show that $HPBW_y$ remains nearly the same when n_x is increased, and similarly the data in Table 3.9 show that $HPBW_x$ changes very little as n_y is increased. Comparison of HPBW values for any given n_x, n_y, and *m* in Tables 3.8 and 3.9 with those in Tables 3.6 and 3.7, respectively, reveals that as the main lobe steers closer to the *xy*-plane, $HPBW_x$ and $HPBW_y$ increase, hence the main lobe broadens in both *x*-*r* and *y*-*r* planes. These results complement the observations made in section 3.1 where the directivity of an array with a fixed size decreased as the elevation angle coordinate of main beam maximum (θ_0) increased.

Table 3.6: Half-power beamwidths $HPBW_x$ and $HPBW_y$ in degrees for planar arrays with $d_x = d_y = \lambda/2$, θ_0 = 0°, and several values of n_x, n_y, and m

$n_x,n_y/m$	2	3	4	5
$HPBW_x$				
5,4	14.941	12.266	10.651	9.5421
6,4	12.367	10.154	8.8181	7.9002
7,4	10.557	8.6691	7.5288	6.7454
8,4	9.2135	7.5661	6.5712	5.8874
9,4	8.1753	6.7138	5.831	5.2243
$HPBW_y$				
5,4	18.915	15.524	13.479	12.074
6,4	18.915	15.524	13.479	12.074
7,4	18.915	15.524	13.479	12.074
8,4	18.915	15.524	13.479	12.074
9,4	18.915	15.524	13.479	12.074

Table 3.7: Half-power beamwidths $HPBW_x$ and $HPBW_y$ in degrees for planar arrays with $d_x = d_y = \lambda/2$, θ_0 = 0°, and several values of n_x, n_v, and m

$n_x,n_y/m$	2	3	4	5
$HPBW_x$				
4,5	18.915	15.524	13.479	12.074
4,6	18.915	15.524	13.479	12.074
4,7	18.915	15.524	13.479	12.074
4,8	18.915	15.524	13.479	12.074
4,9	18.915	15.524	13.479	12.074
$HPBW_y$				
4,5	14.941	12.266	10.651	9.5421
4,6	12.367	10.154	8.8181	7.9002
4,7	10.557	8.6691	7.5288	6.7454
4,8	9.2135	7.5661	6.5712	5.8874
4,9	8.1753	6.7138	5.831	5.2243

Table 3.8: Half-power beamwidths $HPBW_x$ and $HPBW_y$ in degrees for planar arrays with $d_x = d_y = \lambda/2$, θ_0 = 20°, ϕ_0 = 20°, and several values of n_x, n_y, and m

$n_x,n_y/m$	2	3	4	5
$HPBW_x$				
5,4	15.796	12.961	11.252	10.079
6,4	13.069	10.727	9.3142	8.3438
7,4	11.155	9.1573	7.9519	7.1238
8,4	9.7336	7.9917	6.9401	6.2176
9,4	8.636	7.091	6.1582	5.5172
$HPBW_y$				
5,4	19.048	15.631	13.57	12.155
6,4	19.048	15.63	13.568	12.153
7,4	19.047	15.628	13.566	12.151
8,4	19.046	15.626	13.564	12.148
9,4	19.044	15.624	13.561	12.145

Table 3.9: Half-power beamwidths $HPBW_x$ and $HPBW_y$ in degrees for planar arrays with $d_x = d_y = \lambda/2$, θ_0 = 20°, ϕ_0 = 20°, and several values of n_x, n_y, and m

$n_x,n_y/m$	2	3	4	5
$HPBW_x$				
4,5	20.007	16.406	14.238	12.751
4,6	20.001	16.4	14.232	12.745
4,7	19.993	16.393	14.226	12.739
4,8	19.985	16.385	14.218	12.732
4,9	19.975	16.375	14.209	12.723
$HPBW_y$				
4,5	15.045	12.35	10.724	9.607
4,6	12.452	10.224	8.8783	7.954
4,7	10.63	8.7286	7.5803	6.7914
4,8	9.2771	7.6181	6.6162	5.9277
4,9	8.2317	6.7599	5.871	5.2601

Variations of beamwidths $HPBW_x$ and $HPBW_y$ with respect to each of the parameters $\theta_0, \phi_0,\ n_x, n_y,$ and m are plotted as illustrated in Figures 3.5 to 3.16. These plots reveal the extent of the influence of each parameter on $HPBW_x$ and $HPBW_y$ when a single parameter in the set $\{\theta_0, \phi_0, n_x, n_y$ and $m\ \}$ is varied while all the others are kept constant.

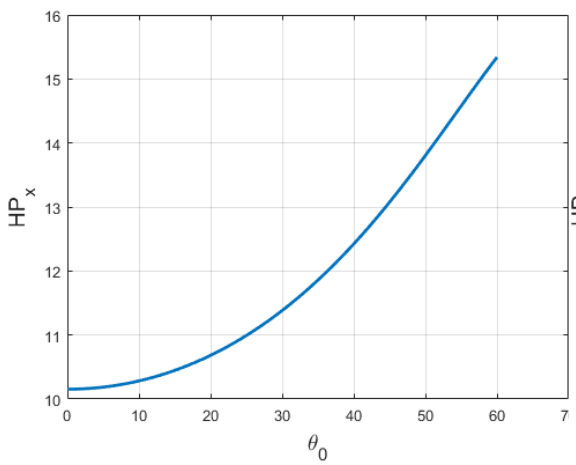

Figure 3.5: Variations of $HPBW_x$ with θ_0 for $\phi_0 = 25°, n_x = 6, n_y = 4, m = 3,$ and $d_x = d_y = \lambda/2$

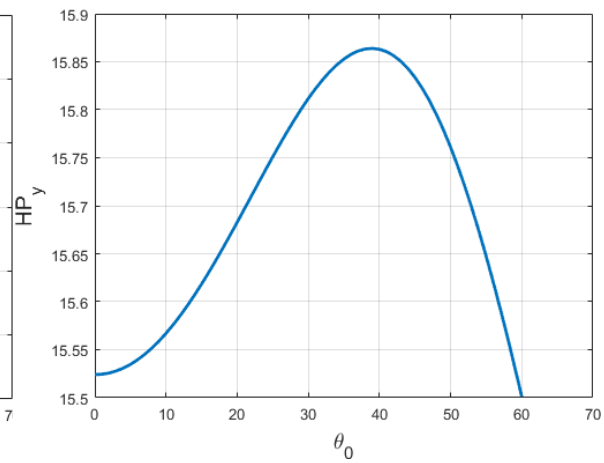

Figure 3.6: Variations of $\mathrm{HPBW_y}$ with θ_0 for $\phi_0 = 25°, n_x = 6, n_y = 4, m = 3,$ and $d_x = d_y = \lambda/2$

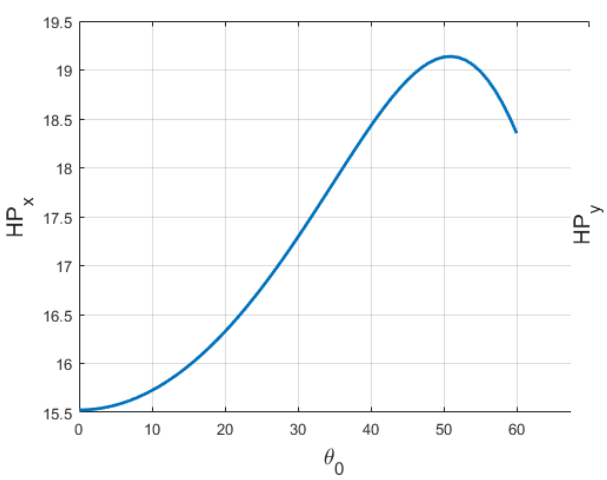

Figure 3.7: Variations of $HPBW_x$ with θ_0 for $\phi_0 = 25°, n_x = 4, n_y = 6, m = 3,$ and $d_x = d_y = \lambda/2$

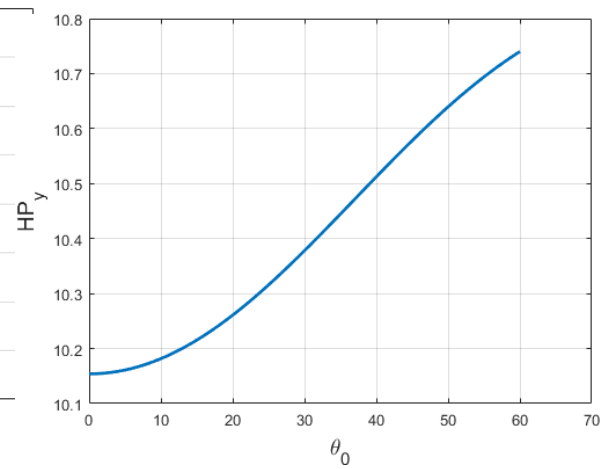

Figure 3.8: Variations of $HPBW_y$ with θ_0 for $\phi_0 = 25°, n_x = 4, n_y = 6, m = 3,$ and $d_x = d_y = \lambda/2$

Figures 3.5 to 3.8 show variations in $HPBW_x$ and $HPBW_y$ when θ_0 is varied from 0° to 60° for given ϕ_0, m, n_x and n_y. Figure 3.5 and 3.6 are for the case when $n_x = 6 > n_y = 4$ whereas Figures 3.7 and 3.8 present beamwidth results when $n_x = 4 < n_y = 6$. Figure 3.5 shows that $HPBW_x$ increases as the elevation angle of the maximum intensity point increases. On the other hand, $HPBW_y$, according to Figure 3.6, first increases and then decreases. The variation in $HPBW_y$ is however negligible. This means that when $n_x > n_y$ as the pattern main lobe steers away from zero elevation angle, it widens in the *x*-*r* plane while the beamwidth in the *y*-*r* plane remains nearly unchanged. Therefore, the decrease in directivity, as observed in Figure 3.3, is as a result of beam broadening in the *x*-*r* plane.

When $n_x < n_y$, Figures 3.7 and 3.8 show that as the elevation angle of the maximum radiation intensity point is increased, $HPBW_y$ increases whereas $HPBW_x$ increases initially and then decreases. The variation in $HPBW_y$ is still negligible, thus it can be said that when the array lattice is rotated 90° about the origin in the *x*-*y* plane, the decrease in directivity would still be due to beam broadening in the *x*-*r* plane.

Figures 3.9 to 3.12 show variations of $HPBW_x$ and $HPBW_y$ with respect to the azimuthal angle ϕ_0 for cases when $n_x = 6 > n_y = 4$ and $n_x = 4 < n_y = 6$. In these figures ϕ_0 is varied from 0° to 90° for given $\theta_0, m, n_x,$ and n_y. Figures 3.9 and 3.10 show that when $n_x > n_y$ and the elevation angle of the maximum radiation intensity point is fixed, as the main lobe is steered in the azimuthal direction, $HPBW_x$ decreases by nearly 1° whereas $HPBW_y$ increases by 1.5°. However, even though the main lobe broadens in the *x*-*r* plane and is narrowed in the *y*-*r* plane, albeit by a little amount, the directivity of the array remains essentially the same as was also observed in Figure 3.2.

Figures 3.11 and 3.12 show that when $n_x < n_y$, $HPBW_x$ decreases by nearly 1.5°, whereas $HPBW_y$ increases by 1° as the array's main beam is steered in the azimuthal direction. The behavior is similar to that noted in Figures 3.9 and 3.10, thereby confirming a similar trait for beamwidth variations with the elevation angle of the main beam peak point: Irrespective of the rectangular array's longer side placed along the *x*-axis or *y*-axis, as the main beam scans in the azimuth plane, it shrinks in the *x*-*r* plane and widens in the *y*-*r* plane. Therefore, the directivity of the array remains nearly unchanged.

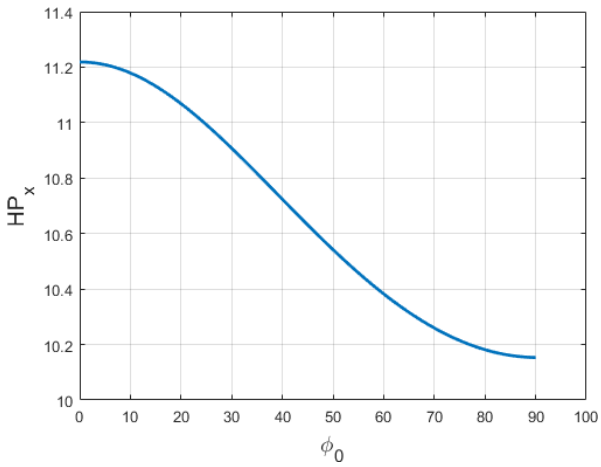

Figure 3.9: Variations of $HPBW_x$ with ϕ_0 for $\theta_0 = 25°, n_x = 6, n_y = 4, m = 3,$ and $d_x = d_y = \lambda/2$

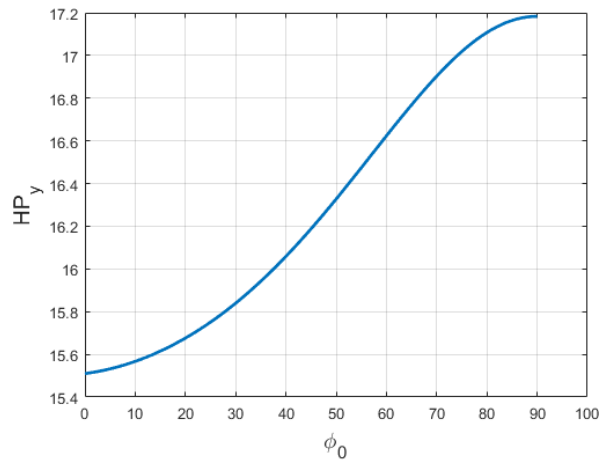

Figure 3.10: Variations of $HPBW_y$ with ϕ_0 for $\theta_0 = 25°, n_x = 6, n_y = 4, m = 3,$ and $d_x = d_y = \lambda/2$

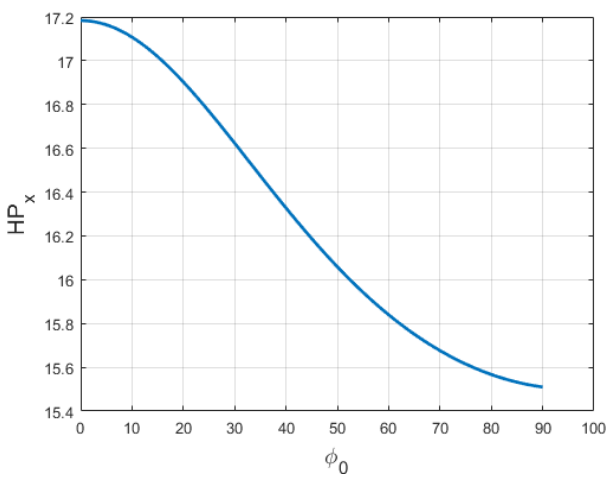

Figure 3.11: Variations of $HPBW_x$ with ϕ_0 for $\theta_0 = 25°, n_x = 4, n_y = 6, m = 3,$ and $d_x = d_y = \lambda/2$

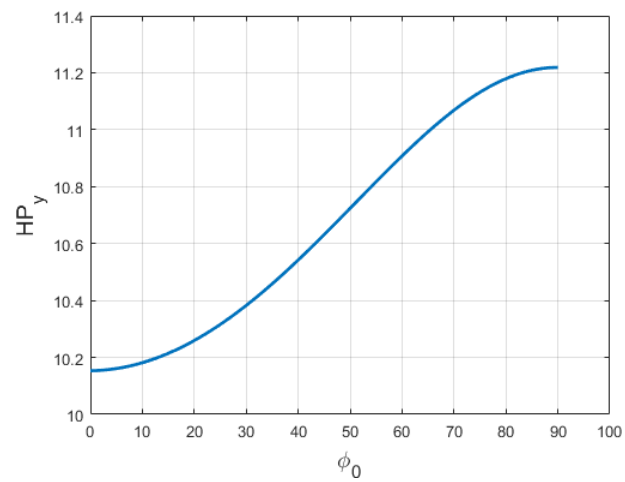

Figure 3.12: Variations of $HPBW_y$ with ϕ_0 for $\theta_0 = 25°, n_x = 4, n_y = 6, m = 3,$ and $d_x = d_y = \lambda/2$

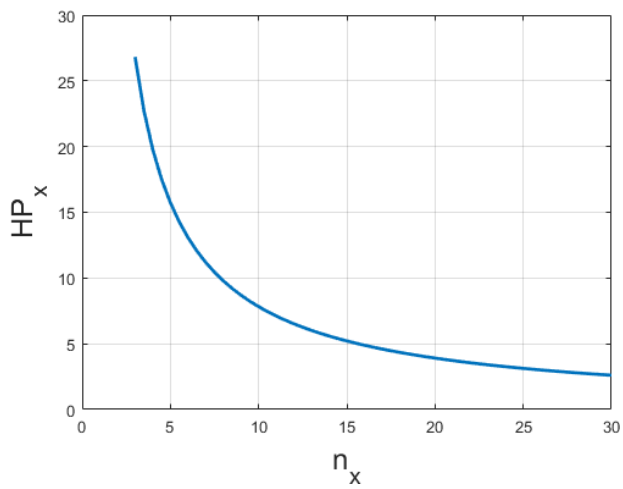

Figure 3.13: Variations of $HPBW_x$ with n_x for $\theta_0 = \phi_0 = 25°$, $n_y = 4$, $m = 3$, and $d_x = d_y = \lambda/2$

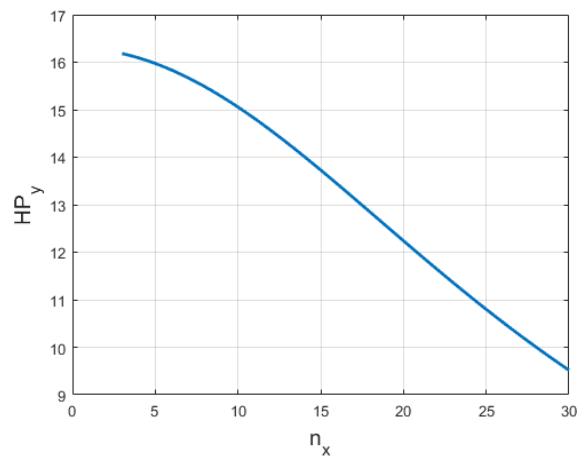

Figure 3.14: Variations of $HPBW$ y with n_x for $\theta_0 = \phi_0 = 25°$, $n_y = 4$, $m = 3$, and $d_x = d_y = \lambda/2$

Figures 3.15 and 3.16 show that both $HPBW_x$ and $HPBW_y$ are decreased when n_y is increased. Therefore, as the length of the rectangular lattice extends along the *y*-axis, narrower beamwidth in both the *x*-*r* and *y*-*r* planes can be achieved at the same boresight. The observation made using Figures 3.13 to 3.16 can be further supported by using Figure 3.3 where the directivity of the array increases significantly as the number of array elements increase along the *x*-axis. This is because as the array elements increase either along the *x* or *y* direction, the main lobe shrinks in both planes thereby, making the radiation pattern more directive.

Figures 3.17 and 3.18 examine variations of $HPBW_x$ and $HPBW_y$ with the exponent *m* when parameters $\theta_0, \phi_0, n_x,$ and n_y are all kept constant. These figures show that both $HPBW_x$ and $HPBW_y$ decrease as *m* increases. Therefore, when the direction of maximum radiation on the main beam is fixed and the rectangular lattice is expanded in both directions through increasing *m*, the main lobe shrinks in both the *x*-*r* and the *y*-*r* planes. The reduction in the two beamwidths manifests itself as higher directivity as observed in Figures 3.1 and 3.2.

In summary, half-power beamwidths of the proposed array are strongly influenced by its size through parameters n_x, n_y, and *m* as well as the direction of maximum radiation.

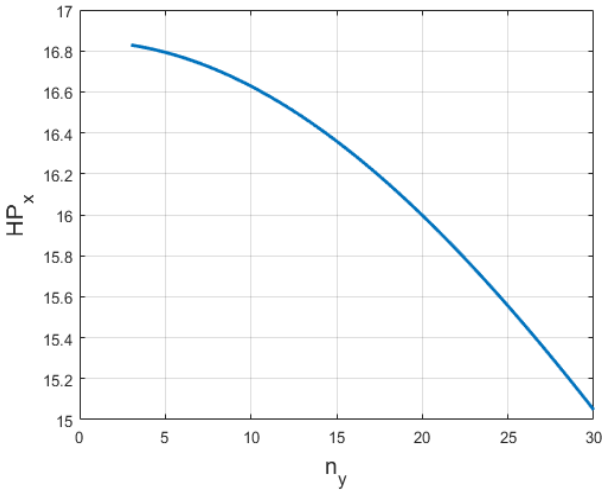

Figure 3.15: Variations of $HPBW_x$ with n_y for $\theta_0 = \phi_0 = 25°$, $n_x = 4$, $m = 3$, and $d_x = d_y = \lambda/2$

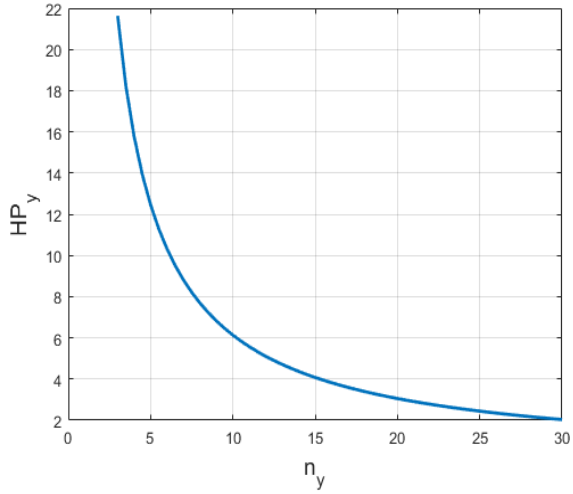

Figure 3.16: Variations of $HPBW_y$ with n_y for $\theta_0 = \phi_0 = 25°$, $n_x = 4$, $m = 3$, and $d_x = d_y = \lambda/2$

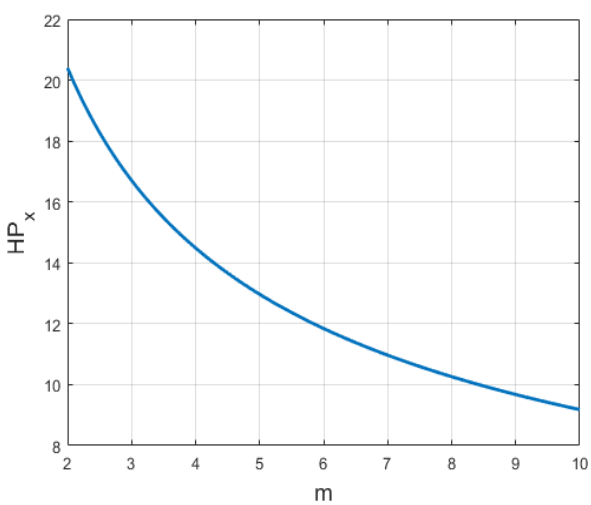

Figure 3.17: Variations of $HPBW_x$ with m for $\theta_0 = \phi_0 = 25°$, $n_x = 8$, $n_y = 4$, and $d_x = d_y = \lambda/2$

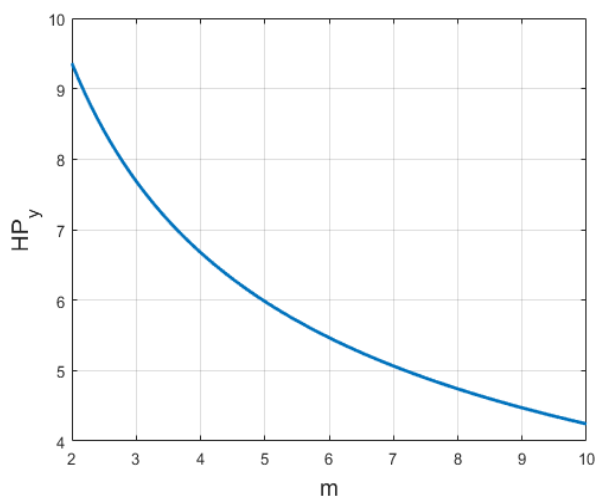

Figure 3.18: Variations of $HPBW_y$ with m for $\theta_0 = \phi_0 = 25°$, $n_x = 8$, $n_y = 4$, and $d_x = d_y = \lambda/2$

3.4 Element Excitation Currents

The geometry of the proposed planar array was described in Chapter 2 and illustrated in Figure 2.1a. This geometry forms the basis of how each element in the array is indexed and its amplitude of excitation computed. As discussed in Section 2.5.3, the number of elements of the array is entirely dependent upon n_x, n_y and m, and once these parameters are known the total number of elements and the excitation coefficient of each element can be computed in a straight forward manner according to (2.44) and (2.45).

In this section, excitation coefficients of the proposed array are calculated, tabulated and analyzed. An insight into the way excitation amplitudes vary across the plane of the array's geometry can reveal practical considerations in feeding the array. One such consideration is the current taper ratio (CTR) defined as the ratio of the maximum excitation coefficient to the minimum excitation coefficient. Knowing the element current distribution of the array can assist in disregarding elements that have relatively lower excitations and contribute little towards the array factor.

It was shown in (2.43) that the array factor for the proposed array can be expressed in terms of summation of excitation coefficients. It was further stated that the element currents for the proposed array can be computed for given values of n_x, n_y and m using (2.43), (2.44) and (2.45). In this section the excitation currents for various values of n_x, n_y and m are calculated and shown in Figures 3.19 (a) – (d). These coefficients are positioned on the *x*-*y* plane with vertical axis on the plane representing the *y*-axis and horizontal axis representing the *x*-axis. The values of n_x, n_y and m are selected such that each possible combination, results in one of the following four possible geometries:

N_x even, N_y even;	N_x even, N_y odd
N_x odd, N_y even;	N_x odd, N_y odd

Figures 3.19 (a) – (d) show element excitations for the above four cases. Figure 3.19 (a) is for an array with $N_x = N_y = 10$ which correspond to $n_x = 4, n_y = 4,$ and $m = 3$. Figure 3.19 (b) – (d) are example cases for

N_x odd, N_y even with $N_x = 10$ and $N_y = 13$ associated with $n_x = 4, n_y = 5,$ and $m = 3$
N_x even, N_y odd with $N_x = 13$ and $N_y = 10$ associated with $n_x = 5, n_y = 4,$ and $m = 3$
N_x odd, N_y odd with $N_x = 13$ and $N_y = 13$ associated with $n_x = 5, n_y = 5,$ and $m = 3$

1	3	6	10	12	12	10	6	3	1
3	9	18	30	36	36	30	18	9	3
6	18	36	60	72	72	60	36	18	6
10	30	60	100	120	120	100	60	30	10
12	36	72	120	144	144	120	72	36	12
12	36	72	120	144	144	120	72	36	12
10	30	60	100	120	120	100	60	30	10
6	18	36	60	72	72	60	36	18	6
3	9	18	30	36	36	30	18	9	3
1	3	6	10	12	12	10	6	3	1

(a)

1	3	6	10	12	12	10	6	3	1
3	9	18	30	36	36	30	18	9	3
6	18	36	60	72	72	60	36	18	6
10	30	60	100	120	120	100	60	30	10
15	45	90	150	180	180	150	90	45	15
18	54	108	180	216	216	180	108	54	18
19	57	114	190	228	228	190	114	57	19
18	54	108	180	216	216	180	108	54	18
15	45	90	150	180	180	150	90	45	15
10	30	60	100	120	120	100	60	30	10
6	18	36	60	72	72	60	36	18	6
3	9	18	30	36	36	30	18	9	3
1	3	6	10	12	12	10	6	3	1

(b)

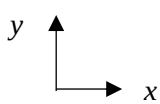

1	3	6	10	15	18	19	18	15	10	6	3	1
3	9	18	30	45	54	57	54	45	30	18	9	3
6	18	36	60	90	108	114	108	90	60	36	18	6
10	30	60	100	150	180	190	180	150	100	60	30	10
12	36	72	120	180	216	228	216	180	120	72	36	12
12	36	72	120	180	216	228	216	180	120	72	36	12
10	30	60	100	150	180	190	180	150	100	60	30	10
6	18	36	60	90	108	114	108	90	60	36	18	6
3	9	18	30	45	54	57	54	45	30	18	9	3
1	3	6	10	15	18	19	18	15	10	6	3	1

(c)

1	3	6	10	15	18	19	18	15	10	6	3	1
3	9	18	30	45	54	57	54	45	30	18	9	3
6	18	36	60	90	108	114	108	90	60	36	18	6
10	30	60	100	150	180	190	180	150	100	60	30	10
15	45	90	150	225	270	285	270	225	150	90	45	15
18	54	108	180	270	324	342	324	270	180	108	54	18
19	57	114	190	285	342	361	342	285	190	114	57	19
18	54	108	180	270	324	342	324	270	180	108	54	18
15	45	90	150	225	270	285	270	225	150	90	45	15
10	30	60	100	150	180	190	180	150	100	60	30	10
6	18	36	60	90	108	114	108	90	60	36	18	6
3	9	18	30	45	54	57	54	45	30	18	9	3
1	3	6	10	15	18	19	18	15	10	6	3	1

(d)

Figure 3.19: Element excitation coefficients for planar arrays with (a) $n_x = 4, n_y = 4\ , m = 3$, (b) $n_x = 4, n_y = 5, m = 3$, (c) $n_x = 5, n_y = 4, m = 3$, (d) $n_x = 5, n_y = 5\ , m = 3$

In general, elements with maximum excitation amplitude are located close to the array center. The excitation amplitude decreases as the elements are traversed from center to *x* or *y* direction. The coefficients also decrease monotonically when traversed diagonally from the center to the corners of the rectangular lattice where the coefficient values are always 1. The symmetry of current distribution with respect to two perpendicular lines parallel to x- and y-axes and passing through the array center is evident from Figures 3.19 (a) - (d). These symmetry properties imply that only about one quarter of element currents actually need be calculated.

3.5 Radiation Patterns

Radiation patterns are three-dimensional polar (or linear if desired) plots of the magnitude of array factor, |AF|, versus spherical coordinates θ and φ. Often a dB scale is used to illustrate the pattern plots where $20\log_{10}$ |AF| instead of |AF| is used. Once the excitation coefficients of elements are determined, (2-46) and (2.47) can be used to simulate and plot the radiation pattern of the array. This method of calculating the array factor is always applicable as long as element currents are known. However, when *m* is an integer, the radiation pattern can be obtained directly from (2.9) in conjunction with (2.7) and (2.8) without need for calculating the element currents.

Radiation patterns for several example cases are presented in this section. Patterns are only shown for the upper half space, namely $0° \leq \theta \leq 90°$ and $0° \leq \varphi \leq 360°$. Figure 3.19 depicts the radiation patterns of an array with $n_x = 6, n_y = 4, m = 2, \phi_0 = 0°$ and several values of θ_0, thus the array size is fixed and the main lobe is steered by varying θ_0. The plots in Figure 3.19 show that when θ_0 is varied from 0° to 60° in 20° steps, the main lobe broadens and consequently the directivity suffers as was also observed in Figure 3.1. Figure 3.19 also shows that as θ_0 increases, more side lobes appear in the radiation pattern and when $\theta_0 = 60°$ the grating lobe emerges. When the grating lobe becomes part of the radiation pattern, the SLL of an array may not be defined analytically based on the SLL analysis presented in Sedction 2.3.2. In such a situation we need to first calculate the array factor at the point on the part of the grating lobe that is included in the patten and assumes

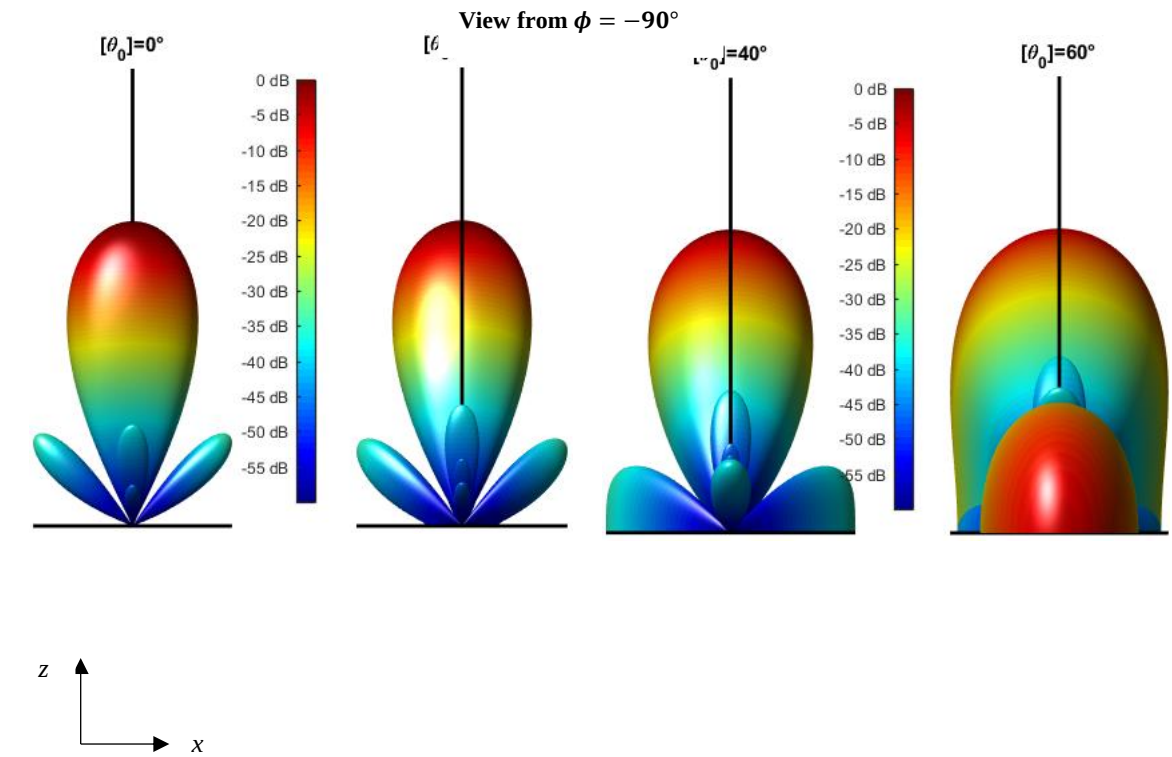

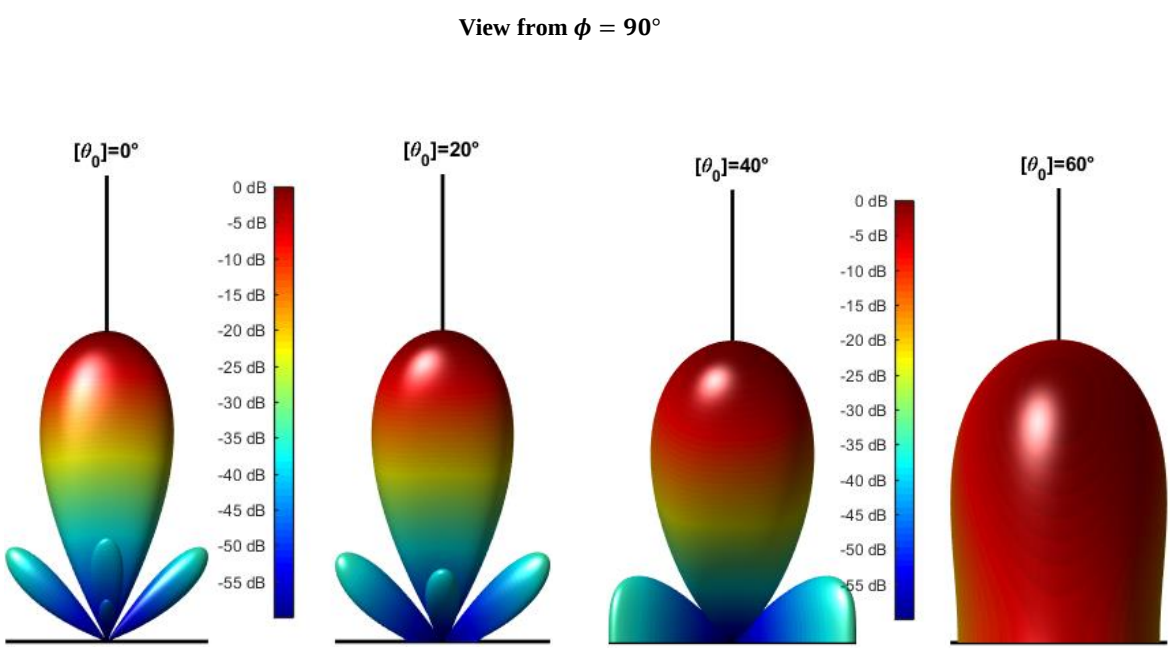

Figure 3.19: Radiation patterns for a planar array with $n_x = 6, n_y = 4, m = 2,$ and $\phi_0 = 0°$

its highest value, then compare it with the SLL value obtained from the side lobe level analysis in Section 2.3.2. The larger of the two values is the correct side lobe level. For $\theta_0 = 60°$ in Figure 3.19, these two values are − 4.7 dB (due to grating lobe) and − 22.6 dB (obtained from SLL abnalysis), thus the correct SLL is indeed − 4.7 dB.

Figure 3.20 illustrates the main lobe of the same array size as Figure 3.19, but steered in the azimuthal direction while the elevation angle of the maximum radiation intensity point is fixed at $\theta_0 = 15°$. It is noted that the steering does not visibly cause any variation in the main lobe, thus confirming the results in Figures 3.9 to 3.12 that variations of $HPBW_x$ and $HPBW_y$ with φ_0 are negligible. The number of side lobes that are greater than − 60 dB also appear to remain roughly the same.

Figure 3.21 depcits the influence of parameter *m* on the main and side lobes of an array with $n_x = 8, n_y = 4, \theta_0 = 15°, \phi_0 = 0°$. The simulations show that as m increases, the number side lobes that are larger than -60 dB reduce significantly. Futhermore, the main lobe exhibits visible flattenening as *m* increases. These simulations validate the conclusions made in Sections 3.1, 3.2 and 3.3 that HPBW and SLL reduce, and the overall directivity increases when *m* increases. However, in order to achieve a pattern that results from *m*=5 in Figure 3.21, 576 elements are required. The pattern for *m*=3, on the other hand, is achieved with just above 300 elements.

Figure 3.22 shows variations in radiation pattern when n_x is varied from 4 to 10 with increments of 2 and for $m = 2, n_y = 4, \theta_0 = 0°, \phi_0 = 0°$. The situation is akin to increasing the array size along the *x*-axis while keeping the boresight fixed in the broadside direction. It can be observed that as n_x increases, $HPBW_x$ appears to reduce while $HPBW_y$ evidently remains the same, thus validating results obtained in Table 3.6. It is also important to note that when the array size is increased along the x axis, more side lobes appear that are also placed along the x axis. However, the number of side lobes located along the y axis remain exactly the same when n_x is increased. This is because the number of side lobes for AF_x (the constituent linear array factor) increase according to $n_x - 2$ and when $n_x = 4, 6, 8$ and 10, the number of side lobes are 2, 4, 6 and 8 respectively. This behaviour is however, more prominent for a broadside array and as the elevation angle

increases, more secondary lobes emerge and the above mentioned relationship between n_x and the number of secondary lobes does not remain valid.

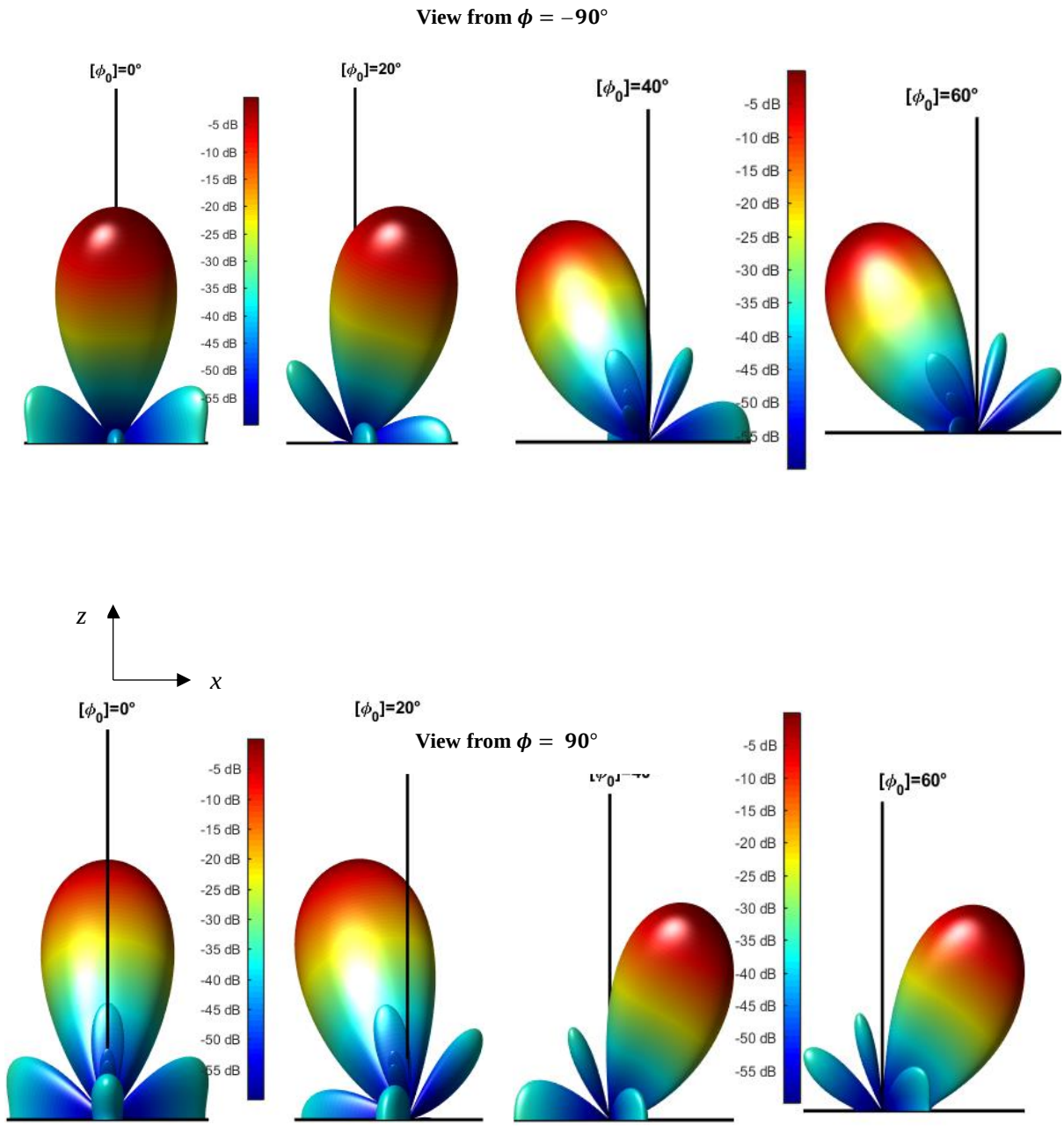

Figure 3.20: Radiation patterns for a planar array with $n_x = 6, n_y = 4, m = 2,$ and $\theta_0 = 15°$

View from $\phi = -90°$

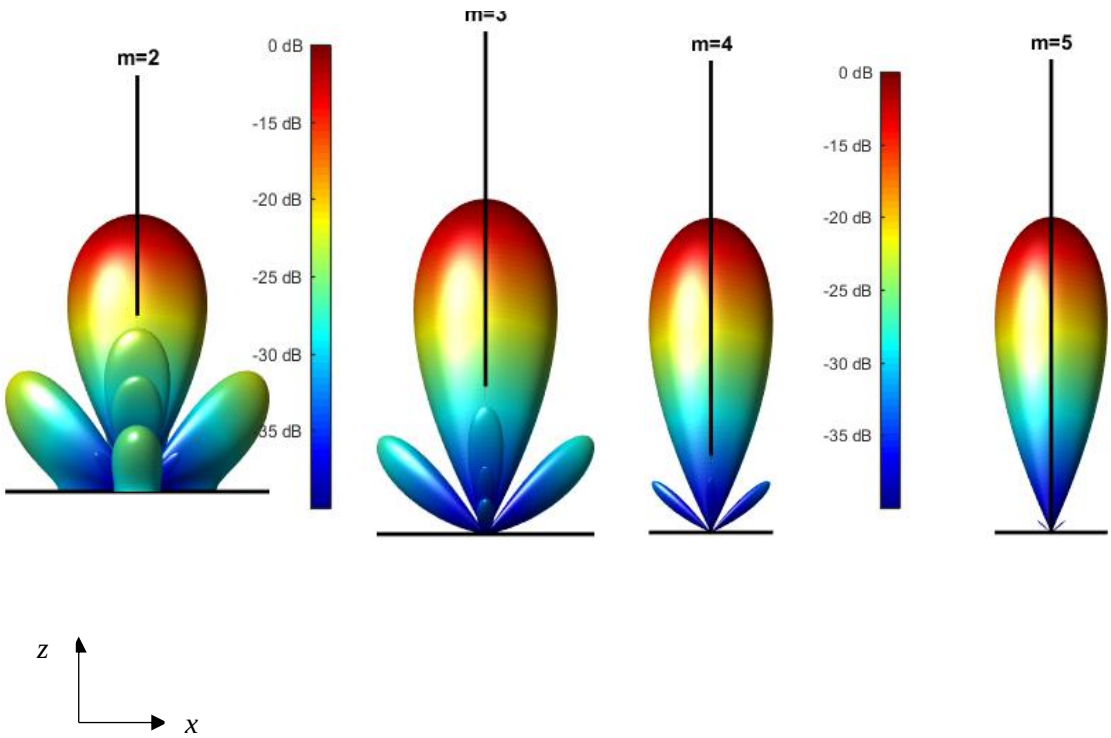

View from $\phi = 45°$

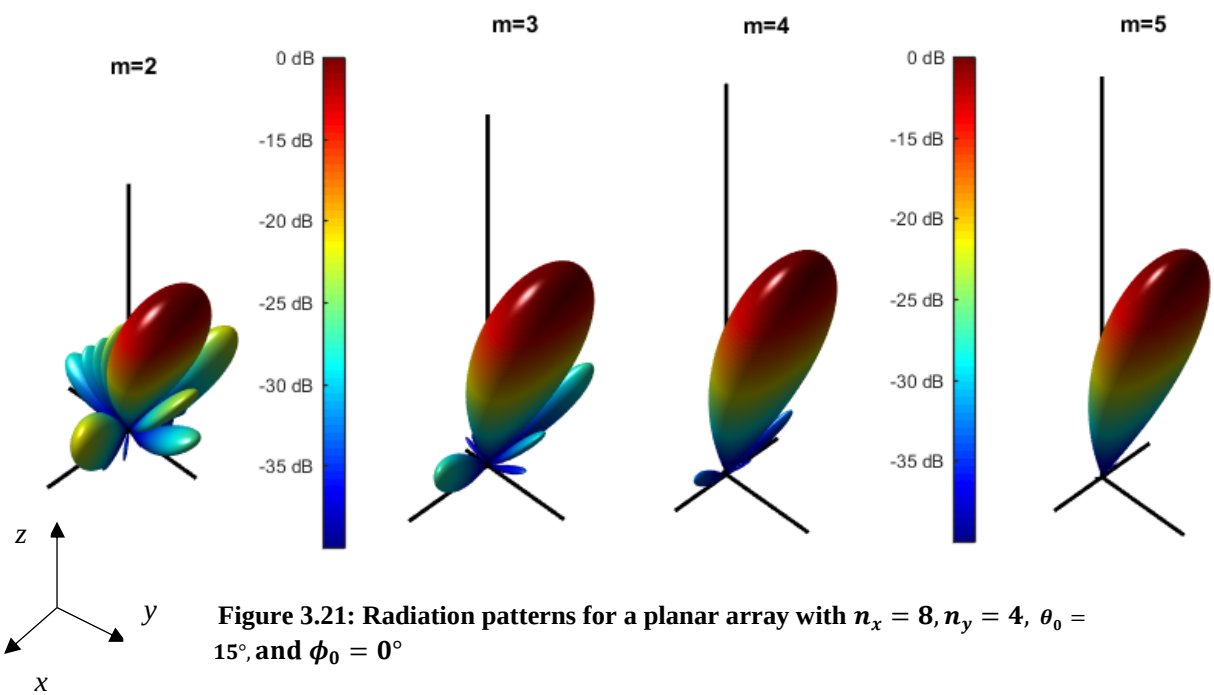

Figure 3.21: Radiation patterns for a planar array with $n_x = 8, n_y = 4$, $\theta_0 = 15°$, and $\phi_0 = 0°$

Radiation pattern as seen from above

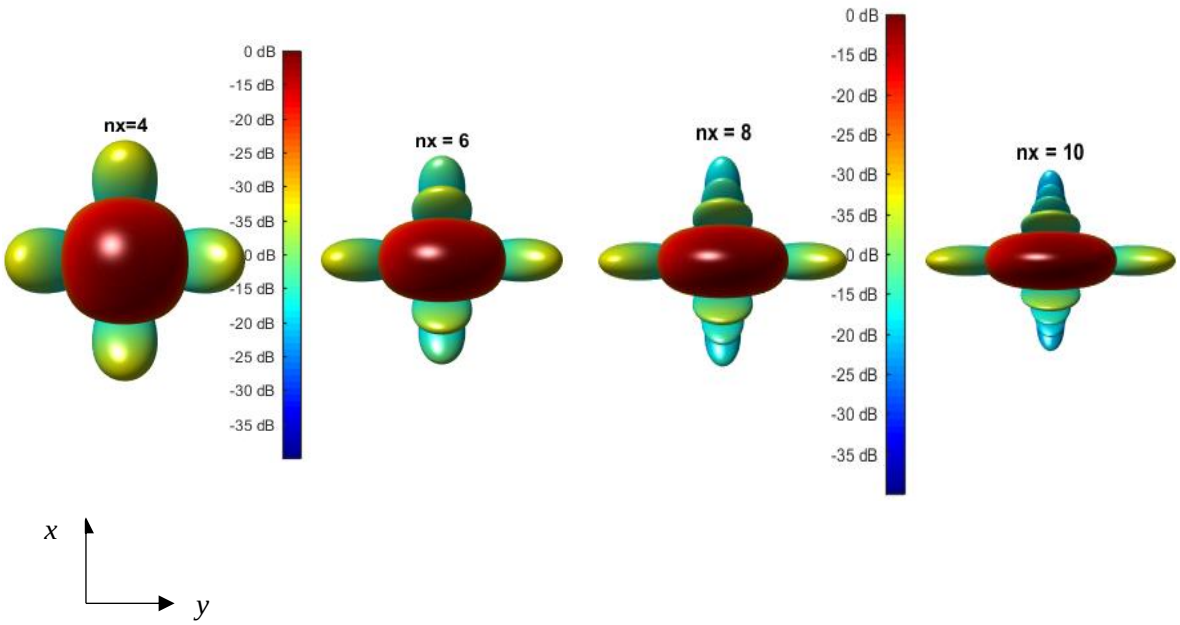

View from $\phi = 135°$

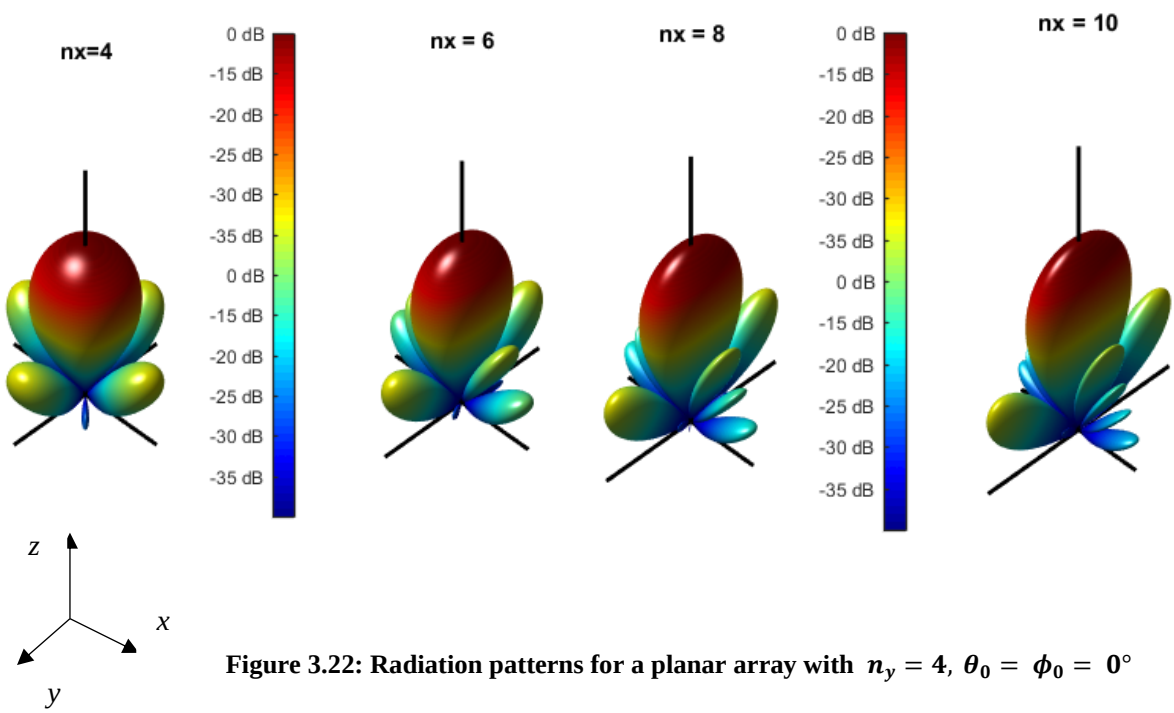

Figure 3.22: Radiation patterns for a planar array with $n_y = 4$, $\theta_0 = \phi_0 = 0°$

Radiation pattern as seen from above

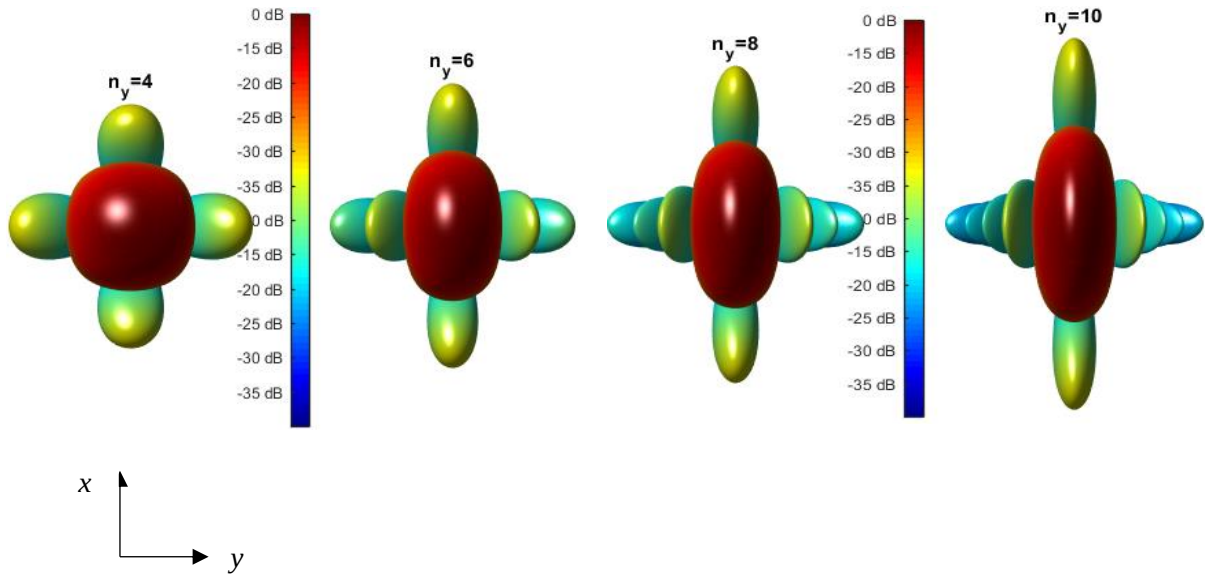

View from $\phi = 135°$

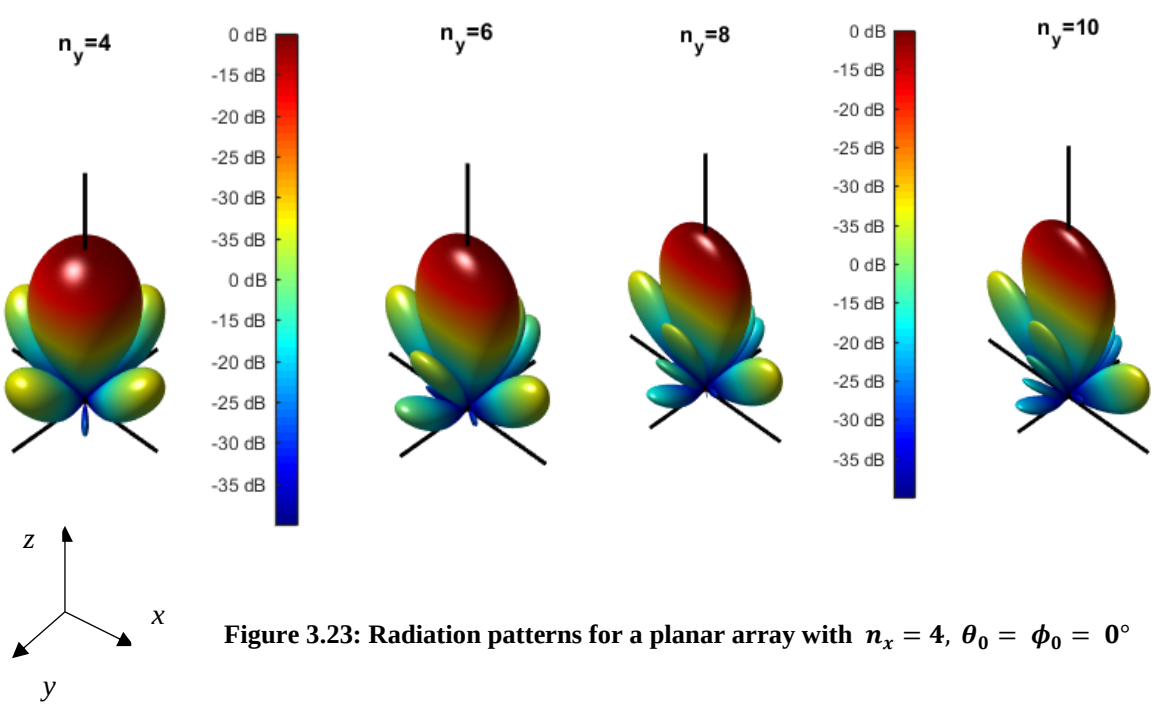

Figure 3.23: Radiation patterns for a planar array with $n_x = 4$, $\theta_0 = \phi_0 = 0°$

Figure 3.23 illustrates variations in radiation pattern when n_y is varied for a planar array with $m = 2, n_x = 4, \theta_0 = 0°, \phi_0 = 0°$. It is noted that as the length of the rectangular lattice is increased along the *y*-axis alone, $HPBW_y$, which lies in the *y*-*z* plane, reduces, thereby confirming the results in Table 3.7. The number of side lobes placed along the *y*-axis increase whereas those along the *x*- axis remains unchanged. This can be explained by analyzing AF_y. For $n_y = 4, 6, 8$ and 10, the number of side lobes are 2, 4, 6 and 8, respectively. Again, this relationship between secondary lobes and n_y is only valid for a boradside pattern.

In summary, this section examined variations of radiation pattern variation with each of the parameters $\theta_0, \phi_0, n_x, n_y$ and m and important trends were identified. Of all the variables, the most significant effect on the array pattern comes from parameter *m*. Increasing *m*, increases directivity significantly while simulatenously reducing HPBW and SLL the most.

3.6 Analysis of Non-integer Value of m

When a non-integer exponent value is used, the series in (2.43) requires infinite number of terms for it to be written in the same form as (2.9). This in turn implies using infinite number of elements to achieve the exact desired pattern. To be able to use the expressions in (2.43) and (2.44), the array factor is approximated by truncating the series of the constituent linear arrays each as having N_x and N_y number of terms respectively. Where N_x and N_y are given as follows

$$N_x = Int.[m(n_x - 1) + 1]$$
$$N_y = Int.[m(n_y - 1) + 1]$$

Int. [.] represents rounding off the values inside the brackets to the nearest integer and the value of m, n_x and n_y used inside the brackets are the exact values. N_x and N_y along with exact value of m, and n_x and n_y rounded to their nearest integer are then used in (2.44) to determine excitation coefficients of the array. The approximated array factor is then determined using (2.46) and (2.47).

3.6.1 Example 1

Determine the array excitation coefficients, directivity, SLL when $n_x = 5, n_y = 4, m = 2.5, \theta_0 = 0° \; and \; \phi_0 = 0°$.

Using the relationships described above, the total number of array elements are determined to be $N_x = 11$ and $N_y = 9$. The excitation coefficients are then calculated using (2.44) and are illustrated in Figure 3.24. It can be observed that when non integer values of *m* are used in such a way, the excitation coefficients of the planar array are also non-integer values. The associated radiation pattern is depicted in Figure 3.25. It should be noted that the approximated array factor is now given by the summation of cosines in (2.46) and (2.47) and not (2.9). The directivity and SLL are computed using these expressions and are found to be 19.39 dB and -27.57 dB respectively. In comparison, if the integer exponent value of *m* = 2 were used, the non-integer *m* of 2.5 gives at least 1.2 dB larger directivity and a SLL that is 4.96 dB smaller.

1	2.5	4.375	6.5625	9.0234	9.2305	9.0234	6.5625	4.375	2.5	1
2.5	6.25	10.938	16.406	22.559	23.076	22.559	16.406	10.938	6.25	2.5
4.375	10.938	19.141	28.711	39.478	40.383	39.478	28.711	19.141	10.938	4.375
6.5625	16.406	28.711	43.066	59.216	60.575	59.216	43.066	28.711	16.406	6.5625
6.5234	16.309	28.54	42.81	58.864	60.214	58.864	42.81	28.54	16.309	6.5234
6.5625	16.406	28.711	43.066	59.216	60.575	59.216	43.066	28.711	16.406	6.5625
4.375	10.938	19.141	28.711	39.478	40.383	39.478	28.711	19.141	10.938	4.375
2.5	6.25	10.938	16.406	22.559	23.076	22.559	16.406	10.938	6.25	2.5
1	2.5	4.375	6.5625	9.0234	9.2305	9.0234	6.5625	4.375	2.5	1

Figure 3.24: Current distribution of the array when $n_x = 5, n_y = 4$ and $m = 2.5, d_x = d_y = \frac{\lambda}{2}, \theta_0 =, \phi_0 = 0°$

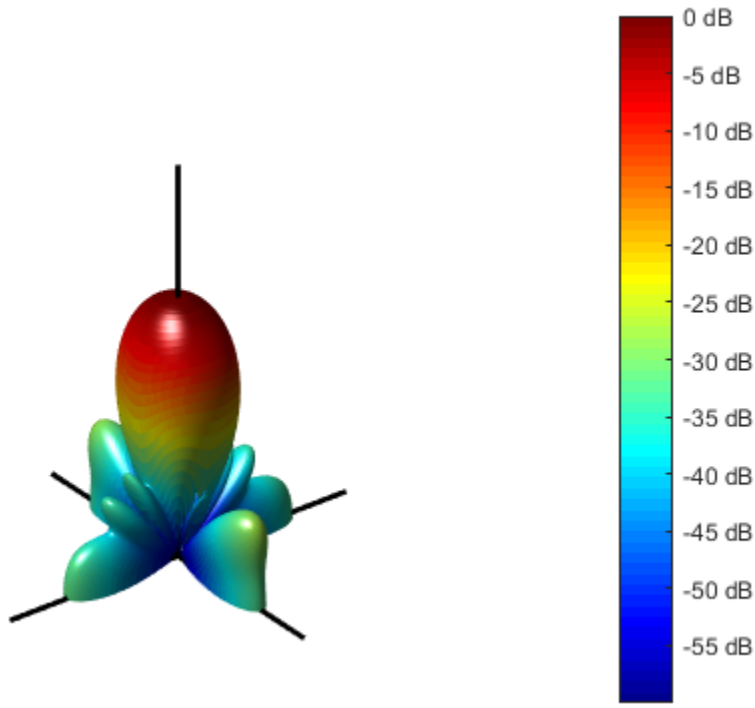

Figure 3.25: Radiation pattern of the array when $n_x = 5, n_y = 4$ and $m = 2.5, d_x = d_y = \frac{\lambda}{2}, \theta_0 = \phi_0 = 0°$

3.6.2 Example 2

Determine the array excitation coefficients, directivity, SLL when $n_x = 6, n_y = 7, m = 2.25, \theta_0 = 15°$ and $\phi_0 = 20°$.

For the above values of n_x, n_y and m, N_x and N_y are determined as 12 and 15 respectively. The excitations of the array are computed in the same manner as in the previous example and are illustrated in Figure 3.26 and the associated radiation pattern in Figure 3.27. It is observed again that for non-integer m, the excitation coefficients are also non integer values. Furthermore, the directivity and SLL are calculated to be 21.92 dB and -26.46 dB respectively. When compared with m =2, the directivity of m = 2.25 is still 0.5 dB larger and the SLL, about 1.61 dB lower.

1	2.25	3.6563	5.1797	6.7983	8.4979	8.4979	6.7983	5.1797	3.6563	2.25	1
2.25	5.0625	8.2266	11.654	15.296	19.12	19.12	15.296	11.654	8.2266	5.0625	2.25
3.6563	8.2266	13.368	18.938	24.856	31.071	31.071	24.856	18.938	13.368	8.2266	3.6563
5.1797	11.654	18.938	26.829	35.213	44.017	44.017	35.213	26.829	18.938	11.654	5.1797
6.7983	15.296	24.856	35.213	46.217	57.772	57.772	46.217	35.213	24.856	15.296	6.7983
8.4979	19.12	31.071	44.017	57.772	72.215	72.215	57.772	44.017	31.071	19.12	8.4979
10.268	23.104	37.544	53.187	69.808	87.259	87.259	69.808	53.187	37.544	23.104	10.268
9.852	22.167	36.021	51.03	66.977	83.721	83.721	66.977	51.03	36.021	22.167	9.852
10.268	23.104	37.544	53.187	69.808	87.259	87.259	69.808	53.187	37.544	23.104	10.268
8.4979	19.12	31.071	44.017	57.772	72.215	72.215	57.772	44.017	31.071	19.12	8.4979
6.7983	15.296	24.856	35.213	46.217	57.772	57.772	46.217	35.213	24.856	15.296	6.7983
5.1797	11.654	18.938	26.829	35.213	44.017	44.017	35.213	26.829	18.938	11.654	5.1797
3.6563	8.2266	13.368	18.938	24.856	31.071	31.071	24.856	18.938	13.368	8.2266	3.6563
2.25	5.0625	8.2266	11.654	15.296	19.12	19.12	15.296	11.654	8.2266	5.0625	2.25
1	2.25	3.6563	5.1797	6.7983	8.4979	8.4979	6.7983	5.1797	3.6563	2.25	1

Figure 3.26: Current distribution of the array when $n_x = 6, n_y = 7$ and $m = 2.25, d_x = d_y = \frac{\lambda}{2}, \theta_0 = 15°, \phi_0 = 20°$

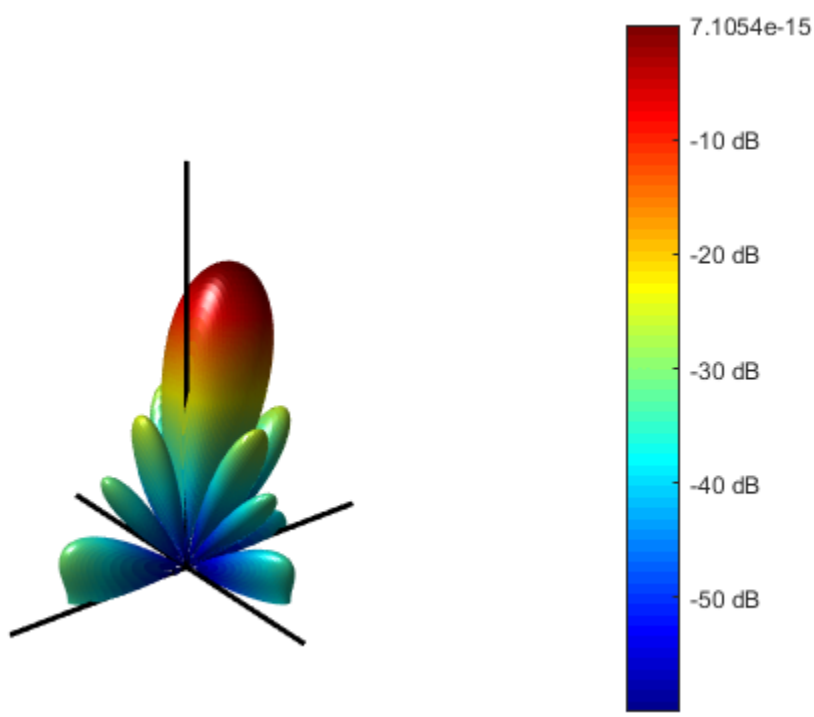

Figure 3.27: Radiation pattern of the array when $n_x = 6, n_y = 7$ and $m = 2.25, d_x = d_y = \frac{\lambda}{2}, \theta_0 = 15°, \phi_0 = 20°$

Chapter 4: Synthesis of Low Side Lobe Planar Arrays

The analytical relationships describing the radiation properties of low side lobe planar arrays were developed in Chapter 2. When the geometry and parameters of the array are defined, its radiation properties, including directivity, half-power beamwidths in the principal planes, side lobe level, and radiation pattern, as well as its element excitation currents can be determined, as was carried out in Chapter 3. This chapter is devoted to synthesis of such arrays for specified design requirements. In particular, a synthesis technique, based on theoretical developments presented in Chapter 2, is sought which produces array designs yielding prescribed side lobe level and half-power beamwidths and a radiation pattern with its main beam maximum along a specified direction in space.

Using the design requirements, the synthesis process should yield the number of array elements, its distribution along the length and width of the array rectangular lattice, and the required element excitation coefficients that produce the desired radiation pattern properties. The design requirements amount to specified values for SLL, $HPBW_x$, $HPBW_y$, θ_0, ϕ_0, d_x, and d_y, which are used in equations governing the radiation characteristics of the array to determine the parameters n_x, n_y, m, and element excitation coefficients as the synthesis outcome.

4.1 Synthesis Procedure

The side lobe level equation (2.10) together with two half-power beamwidth relations (2.29) and (2.30) constitute the main synthesis equations which are solved simultaneously to determine the design parameters n_x, n_y, and m. From a mathematical point of view the above equations can be thought of as a system of three equations and three unknowns. These equations and their dependence on the unknowns n_x, n_y, and m are of a complex nature and solving them simultaneously can be facilitated by further developments as described below.

From half-power beamwidth equations (2.29) and (2.30), it is readily concluded that

$$\left|\frac{\sin\left(\frac{n_x\psi_{HPx}}{2}\right)}{n_x\sin\left(\frac{\psi_{HPx}}{2}\right)}\cdot\frac{\sin\left(\frac{n_y\overline{\psi}_{HPx}}{2}\right)}{n_y\sin\left(\frac{\overline{\psi}_{HPx}}{2}\right)}\right| = \left|\frac{\sin\left(\frac{n_x\overline{\psi}_{HPy}}{2}\right)}{n_x\sin\left(\frac{\overline{\psi}_{HPy}}{2}\right)}\cdot\frac{\sin\left(\frac{n_y\psi_{HPy}}{2}\right)}{n_y\sin\left(\frac{\psi_{HPy}}{2}\right)}\right|$$

which upon rearranging the terms is written as

$$\left|\sin\left(\frac{n_x\psi_{HPx}}{2}\right)\right|\left|\sin\left(\frac{n_y\overline{\psi}_{HPx}}{2}\right)\right|\left|\sin\left(\frac{\overline{\psi}_{HPy}}{2}\right)\right|\left|\sin\left(\frac{\psi_{HPy}}{2}\right)\right| - \left|\sin\left(\frac{n_x\overline{\psi}_{HPy}}{2}\right)\right|\left|\sin\left(\frac{n_y\psi_{HPy}}{2}\right)\right|\left|\sin\left(\frac{\psi_{HPx}}{2}\right)\right|\left|\sin\left(\frac{\overline{\psi}_{HPx}}{2}\right)\right| = 0 \qquad (4.1)$$

where ψ_{HPx}, ψ_{HPy}, $\overline{\psi}_{HPx}$, and $\overline{\psi}_{HPy}$ are given by (2.31), (2.32), (2.35), and (2.36), respectively. Equation (4.1) is dependent upon only n_x and n_y and thus can be symbolically expressed as

$$f_1(n_x, n_y) = 0 \qquad (4.2)$$

Next, using the side lobe level equation (2.10), the parameter *m* is calculated as

$$m = \frac{SLL_{dB}}{20} / \log_{10}\left|\frac{\sin\left(\frac{n\psi_{SLL}}{2}\right)}{n\sin\left(\frac{\psi_{SLL}}{2}\right)}\right| \qquad (4.3)$$

where

$$n = \begin{cases} n_x\,, & HPBW_y < HPBW_x \\ n_y\,, & HPBW_y > HPBW_x \end{cases} \qquad (4.4a)$$

$$\psi_{SLL} = \begin{cases} \psi_{SLLx}\,, & HPBW_y < HPBW_x \\ \psi_{SLLy}\,, & HPBW_y > HPBW_x \end{cases} \qquad (4.4b)$$

Now taking the log of both sides (2.29), yields

$$\log_{10}\left|\frac{\sin\left(\frac{n_x\psi_{HPx}}{2}\right)}{n_x\sin\left(\frac{\psi_{HPx}}{2}\right)}\cdot\frac{\sin\left(\frac{n_y\overline{\psi}_{HPx}}{2}\right)}{n_y\sin\left(\frac{\overline{\psi}_{HPx}}{2}\right)}\right| + \frac{\log_{10}2}{2m} = 0 \qquad (4.5)$$

Substituting for *m* from (4.3) in (4.5), we obtain

$$\log_{10}\left|\frac{\sin\left(\frac{n_x\psi_{HPx}}{2}\right)}{n_x\sin\left(\frac{\psi_{HPx}}{2}\right)}\cdot\frac{\sin\left(\frac{n_y\overline{\psi}_{HPx}}{2}\right)}{n_y\sin\left(\frac{\overline{\psi}_{HPx}}{2}\right)}\right|+\frac{10\log_{10}2}{SLL_{dB}}\cdot\log_{10}\left|\frac{\sin\left(\frac{n\psi_{SLL}}{2}\right)}{n\sin\left(\frac{\psi_{SLL}}{2}\right)}\right|=0$$

which upon performing inverse log and rearranging the terms is expressed as

$$\left|n\sin\left(\frac{n\psi_{SLL}}{2}\right)\right|^{\gamma}\left|n_x\sin\left(\frac{\psi_{HPx}}{2}\right)\ n_y\sin\left(\frac{\overline{\psi}_{HPx}}{2}\right)\right|+$$
$$\left|n\sin\left(\frac{\psi_{SLL}}{2}\right)\right|^{\gamma}\left|\sin\left(\frac{n_x\psi_{HPx}}{2}\right)\sin\left(\frac{n_y\overline{\psi}_{HPx}}{2}\right)\right|=0 \qquad (4.6)$$

where $\gamma=-\frac{10\log_{10}2}{SLL_{dB}}$.

Equation (4.6) is also dependent upon only n_x and n_y and thus may be written as

$$f_2(n_x,n_y)=0 \qquad (4.7)$$

Equations (4.2) and (4.7) are regarded as a system of two equations and two unknowns. For known values of SLL, $HPBW_x, HPBW_y$, θ_0, ϕ_0, d_x, and d_y, they are solved numerically for n_x and n_y. It must be noted that n_x and n_y are the number of linear array elements of NUELA and can only be positive integers. Therefore, n_x and n_y are rounded off to the nearest integers. Once n_x and n_y have been determined, m is calculated from (4.3) or (4.5). The parameter m is a positive real number which may or may not be an integer. However, for the purpose of this study, only integer values of m are considered and accordingly the solution of m is also rounded off to the nearest integer.

4.2 Design Examples

In this section, the syntheses procedure is validated by designing planar arrays for given values of side lobe level, half-power beamwidths, and boresight angles. The element spacing is assumed to be one-half wavelength for all cases studied. It is further examined whether the determined values of n_x, n_y and m using the procedure described above indeed result in the desired radiation pattern requirements.

The desired input design data is given by $HPBW_x^{(1)}, HPBW_y^{(1)}$ and $SLL^{(1)}$ and the corresponding values of n_x, n_y and m are determined. These values are then used to

determine the total number of array elements and the excitation amplitude of the currents for each element. To verify if the calculated values of n_x, n_y and m produce results that are close to the design input data, they are substituted in (2.10), (3.1) and (3.2) and corresponding values of $HPBW_x^{(2)}, HPBW_y^{(2)}$ and $SLL^{(2)}$ are calculated. As a final step $HPBW_x^{(1)}, HPBW_y^{(1)}$ and $SLL^{(1)}$ are compared with $HPBW_x^{(2)}, HPBW_y^{(2)}$ and $SLL^{(2)}$.

4.2.1 Design Example 1:

Design an array that satisfies the following radiation pattern requirements:

$HPBW_x^{(1)} = 15°, HPBW_y^{(1)} = 12.5°, SLL^{(1)} = -24$ dB and the maximum radiation intensity in the direction $\theta_0 = \phi_0 = 0°$

For this example, $HPBW_x^{(1)} > HPBW_y^{(1)}$ thus $\psi_{SLL} = \psi_{SLL}^x$ and $n = n_x$ are used. The solutions for n_x and n_y are obtained by solving (4.1) and (4.6) simultaneously. Since these equations are nonlinear, it is easier to achieve a solution by substituting possible values of n_x in both (4.1) and (4.6) and finding corresponding solutions of n_y.The set of solutions $\{n_{x1}, n_{y1}\}$ for (4.1) and $\{n_{x2}, n_{y2}\}$ for (4.6) are plotted in Figure 4.1(a). The intersection of $\{n_{x1}, n_{y1}\}$ and $\{n_{x2}, n_{y2}\}$ satisfies (4.1) and (4.6) simultaneously and it is determined to be at $n_x = 5$ and $n_y = 6$ in Figure 4.1(a). Next, using (4.3) it is found out that $m = 2$. For these values, the number of elements placed along the x and y directions are $N_x = 9$ and $N_y = 11$ respectively, and the total number of elements in the array is 99. Furthermore, condition (2.22) is satisfied for n_x determined above and a real $\theta = 33.3°$ exists at which SLL can be defined analytically. The current distribution required to achieve the pattern requirements is found using (2.44) and is illustrated in Figure 4.1(b). The associated radiation pattern is depicted in Figure 4.1(c). The calculated results are then used to compute $HPBW_x^{(2)}, HPBW_y^{(2)}$ and $SLL^{(2)}$. Table 4.1 shows that the computed values are considerably close to the desired requirements.

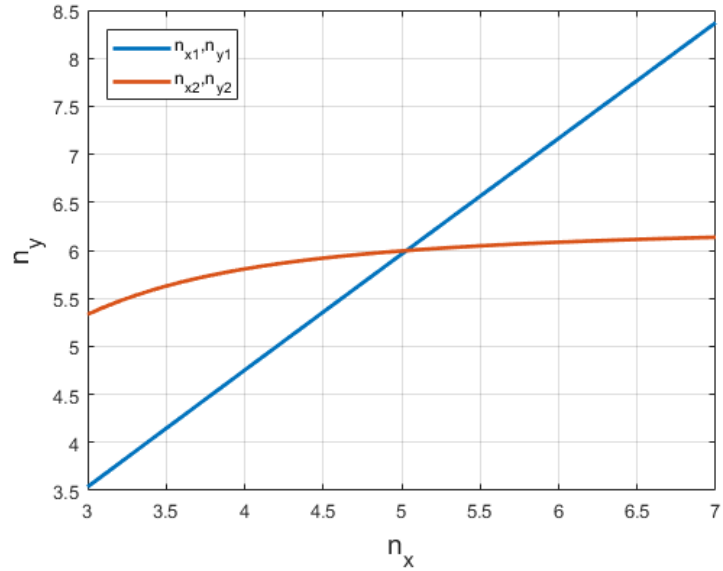

Figure 4.1 (a): Solution space for n_x *and* n_y when $HPBW_x^{(1)} = 15°, HPBW_y^{(1)} = 12.5°, SLL^{(1)} = -24$ dB and $\theta_0 = \phi_0 = 0°$

1	2	3	4	5	4	3	2	1
2	4	6	8	10	8	6	4	2
3	6	9	12	15	12	9	6	3
4	8	12	16	20	16	12	8	4
5	10	15	20	25	20	15	10	5
6	12	18	24	30	24	18	12	6
5	10	15	20	25	20	15	10	5
4	8	12	16	20	16	12	8	4
3	6	9	12	15	12	9	6	3
2	4	6	8	10	8	6	4	2
1	2	3	4	5	4	3	2	1

Figure 4.1 (b): Current distribution of the designed array when $n_x = 5, n_y = 6$ and $m = 2$

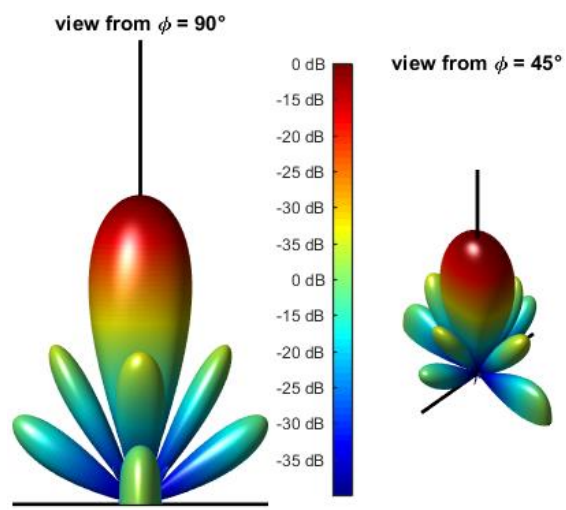

Figure 4.1 (c): Radiation Pattern of the designed array when $n_x = 5, n_y = 6$ and $m = 2$

Table 4.1: Comparison of design requirements with achieved characteristics

$HPBW_x^{(1)}$	$HPBW_x^{(2)}$	$HPBW_y^{(1)}$	$HPBW_y^{(2)}$	$SLL^{(1)}$[dB]	$SLL^{(2)}$[dB]
15°	14.94°	12.5°	12.37°	−24	−24.08

4.2.2 Design Example 2:

Design an array that satisfies the following radiation pattern requirements:

$HPBW_x^{(1)} = 12.5°, HPBW_y^{(1)} = 10°, SLL^{(1)} = -25$ dB for a boresight at $\theta_0 = 15°$ and $\phi_0 = 20°$

Again, $HPBW_x > HPBW_y$ and $\psi_{SLL} = \psi_{SLL}^x$ and $n = n_x$ should be used. The solution set $\{n_{x1}, n_{y1}\}$ and $\{n_{x2}, n_{y2}\}$, as depicted in Figure 4.2(a), intersect at $n_x = 6.16, n_y = 7.46$ for which $m = 1.97$. After rounding off to the nearest integer, we get $n_x = 6, n_y = 7$. The array is designed for both $m = 2$ and $m = 1.97$.

When m =2, $n_x = 6$, and $n_y = 7$ we have $N_x = 11, N_y = 13$, whereas for m =1.97, $n_x = 6.16$, and $n_y = 7.46$, the values of N_x and N_y are determined as 11 and 14 respectively. The total number of elements for integer *m* is 143 whereas for non-integer m, 154 elements are obtained.

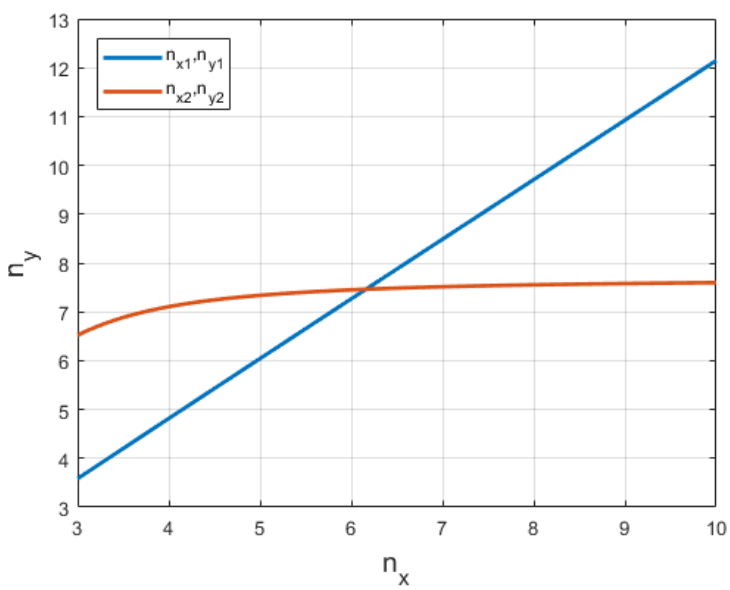

Figure 4.2 (a): Solution space for n_x and n_y when $HPBW_x^{(1)} = 12.5°, HPBW_y^{(1)} = 10°, SLL^{(1)} = -25$ dB and $\theta_0 = 15, \phi_0 = 20°$

1	2	3	4	5	6	5	4	3	2	1
2	4	6	8	10	12	10	8	6	4	2
3	6	9	12	15	18	15	12	9	6	3
4	8	12	16	20	24	20	16	12	8	4
5	10	15	20	25	30	25	20	15	10	5
6	12	18	24	30	36	30	24	18	12	6
7	14	21	28	35	42	35	28	21	14	7
6	12	18	24	30	36	30	24	18	12	6
5	10	15	20	25	30	25	20	15	10	5
4	8	12	16	20	24	20	16	12	8	4
3	6	9	12	15	18	15	12	9	6	3
2	4	6	8	10	12	10	8	6	4	2
1	2	3	4	5	6	5	4	3	2	1

Figure 4.2 (b): Current distribution of the designed array when $n_x = 6, n_y = 7$ and $m = 2$

1	1.97	2.9254	3.8713	4.8101	5.7433	4.8101	3.8713	2.9254	1.97	1
1.97	3.8809	5.7631	7.6266	9.476	11.314	9.476	7.6266	5.7631	3.8809	1.97
2.9254	5.7631	8.5583	11.325	14.072	16.802	14.072	11.325	8.5583	5.7631	2.9254
3.8713	7.6266	11.325	14.987	18.622	22.234	18.622	14.987	11.325	7.6266	3.8713
4.8101	9.476	14.072	18.622	23.138	27.626	23.138	18.622	14.072	9.476	4.8101
5.7433	11.314	16.802	22.234	27.626	32.986	27.626	22.234	16.802	11.314	5.7433
6.6718	13.143	19.518	25.829	32.092	38.318	32.092	25.829	19.518	13.143	6.6718
6.6718	13.143	19.518	25.829	32.092	38.318	32.092	25.829	19.518	13.143	6.6718
5.7433	11.314	16.802	22.234	27.626	32.986	27.626	22.234	16.802	11.314	5.7433
4.8101	9.476	14.072	18.622	23.138	27.626	23.138	18.622	14.072	9.476	4.8101
3.8713	7.6266	11.325	14.987	18.622	22.234	18.622	14.987	11.325	7.6266	3.8713
2.9254	5.7631	8.5583	11.325	14.072	16.802	14.072	11.325	8.5583	5.7631	2.9254
1.97	3.8809	5.7631	7.6266	9.476	11.314	9.476	7.6266	5.7631	3.8809	1.97
1	1.97	2.9254	3.8713	4.8101	5.7433	4.8101	3.8713	2.9254	1.97	1

Figure 4.2 (c): Current distribution of the designed array when $n_x = 6, n_y = 7$ and $m = 1.97$

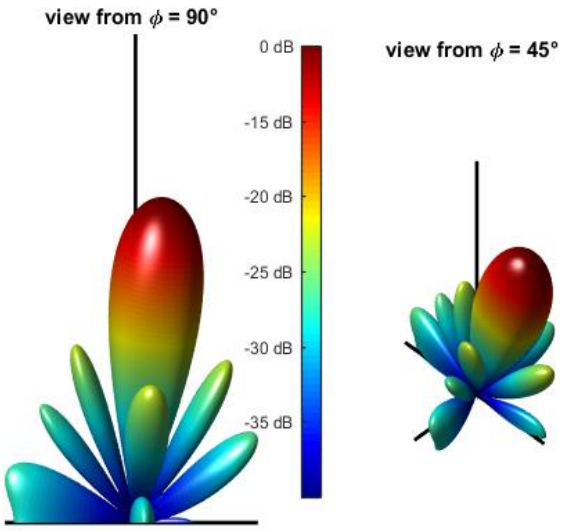

Figure 4.2 (d): Radiation Pattern of the designed array when $n_x = 6, n_y = 7$ and $m = 2$

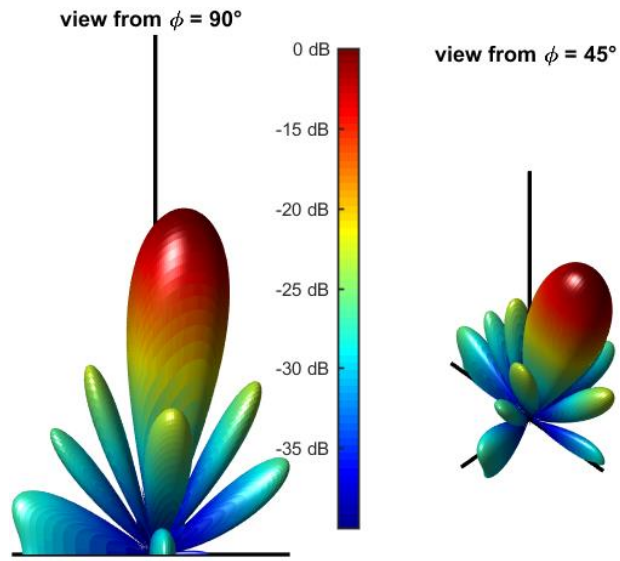

Figure 4.2 (e): Radiation Pattern of the designed array when $n_x = 6, n_y = 7$ and $m = 1.97$

Table 4.2: Comparison of design requirements with achieved characteristics

m	$HPBW_x^{(1)}$	$HPBW_x^{(2)}$	$HPBW_y^{(1)}$	$HPBW_y^{(2)}$	$SLL^{(1)}$ [dB]	$SLL^{(2)}$ [dB]	D [dB]
2	12.5°	12.75°	10°	10.6°	−25	−24.85	21.41
1.97	12.5°	12.66°	10°	10.52°	−25	−24.82	21.49

A real value of θ exists according to condition (2.22) and SLL can be determined analytically. The excitation coefficients for the integer m = 2 is illustrated in Figure 4.2 (b) and for m = 1.97, in Figure 4.2 (c). The associated radiation patterns are depicted in Figure 4.2 (d) and Figure 4.2(e) respectively.

Parameters including $HPBW_x, HPBW_y$, SLL and directivity are calculated for both integer and non-integer m and are documented in Table 4.2. It is clear thatfor the designed array, $HPBW_x, HPBW_y$ and SLL differ from the required values by 0.25°, 0.6 ° and -0.15 dB, respectively when m =2 is used in calculations. Whereas for m = 1.97, the above parameters differ by 0.16°, 0.52 ° and -0.16 dB, respectively.

Comparison between integer and non-integer m in Table 4.2 also reveals that for m = 1.97, $HPBW_x$ and $HPBW_y$ are both smaller when compared to their counterparts from m = 2. Consequently, the directivity of the array resulting from m = 1.97 is larger than that from

m = 2 by an order of 0.09 dB. Furthermore, the SLL for m = 1.97 is roughly the same as that of m = 2.

4.2.3 Design Example 3:

Design an array that satisfies the following radiation pattern requirements:

$HPBW_y^{(1)} = 15°, HPBW_x^{(1)} = 12.5°, SLL^{(1)} = -35$ dB for a boresight at $\theta_0 15°$ and $\phi_0 = 20°$

For the above case, $HPBW_y^{(1)} > HPBW_x^{(1)}$ thus $\psi_{SLL} = \psi_{SLL}^y$ and $n = n_y$ are used. The values of n_x and n_y are obtained by solving (4.1) and (4.8) simultaneously where the solution sets $\{n_{x1}, n_{y1}\}$ and $\{n_{x2}, n_{y2}\}$ correspond to (4.1) and (4.8) respectively. The intersection point using Figure 4.3 (a) if found to be $n_x = 5.1$ and $n_y = 4.1$ for which $m = 3.09$. After rounding off to the nearest integer, $n_x = 5, n_y = 4$ and $m = 3$ are obtained

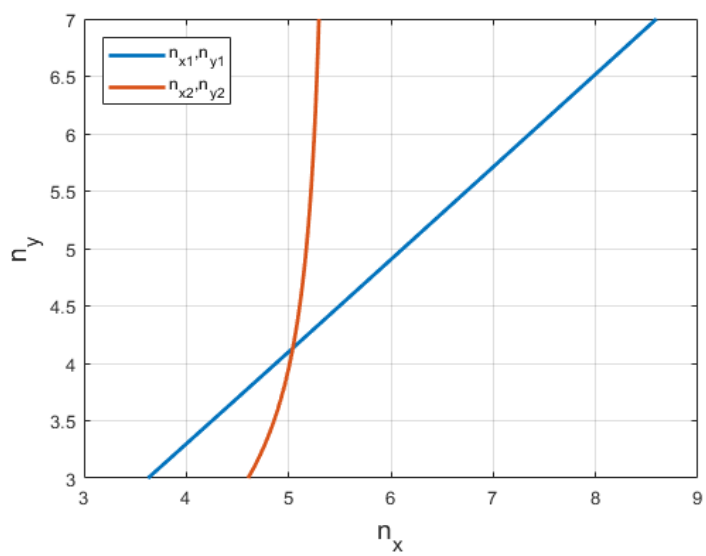

Figure 4.3 (a): Solution space for n_x and n_y when $HPBW_x^{(1)} = 12.5°, HPBW_y^{(1)} = 15°, SLL^{(1)} = -35$ dB and $\theta_0 = 15, \phi_0 = 20°$

1	3	6	10	15	18	19	18	15	10	6	3	1
3	9	18	30	45	54	57	54	45	30	18	9	3
6	18	36	60	90	108	114	108	90	60	36	18	6
10	30	60	100	150	180	190	180	150	100	60	30	10
12	36	72	120	180	216	228	216	180	120	72	36	12
12	36	72	120	180	216	228	216	180	120	72	36	12
10	30	60	100	150	180	190	180	150	100	60	30	10
6	18	36	60	90	108	114	108	90	60	36	18	6
3	9	18	30	45	54	57	54	45	30	18	9	3
1	3	6	10	15	18	19	18	15	10	6	3	1

Figure 4.3 (b): Current distribution of the designed array when $n_x = 5, n_y = 4$ and $m = 3$

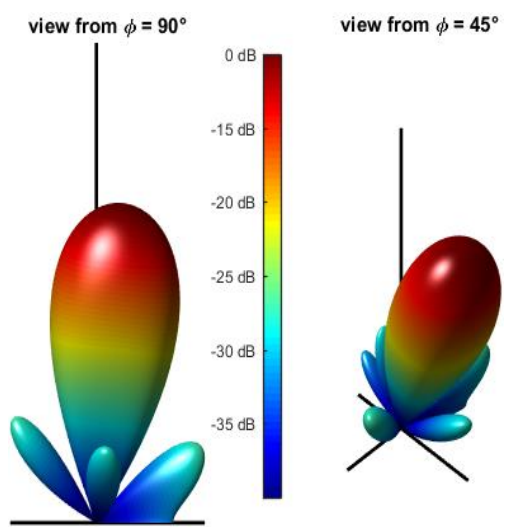

Figure 4.3 (c): Radiation Pattern of the designed array when $n_x = 5, n_y = 4$ and $m = 3$

Table 4.3: Comparison of design requirements with achieved characteristics

$HPBW_x^{(1)}$	$HPBW_x^{(2)}$	$HPBW_y^{(1)}$	$HPBW_y^{(2)}$	$SLL^{(1)}$[dB]	$SLL^{(2)}$[dB]
12.5°	12.65°	15°	15.6°	−35	−34

for which $N_x = 13, N_y = 10$ and $N_{total} = 130$. Furthermore, condition (2.22) is checked is found to be valid for this boresight. The array excitation coefficients for the array are illustrated in Figure 4.3(b) and the related radiation pattern is shown in Figure 4.3(c). The desired and calculated radiation pattern characteristics are compared in Table 4.

4.2.4 Design Example 4:

Design an array that satisfies the following radiation pattern requirements:

$HPBW_y^{(1)} = 9.5°, HPBW_x^{(1)} = 7.5°, SLL^{(1)} = -40$ dB for a boresight at $\theta_0 = 25°$, and $\phi_0 = 90°$

Using a similar procedure as discussed in the preceding examples, values of $n_x = 8$ and $n_y = 7$ are determined using Figure 4.4 (a) for which the associated value of m is 3. The number of elements along the x and y axes are $N_x = 22$ and $N_y = 19$ respectively whereas $N_{total} = 418$. The associated excitation coefficients in Figure 4.4 (b) will result in the radiation pattern of 4.4 (c). The HPBWs and SLL of the pattern in 4.4(c) are also compared with the required values in Table 4.4 and shows a deviation of $0.06°, 0.07°$ and 2dB in $HPBW_x, HPBW_y$ and SLL respectively.

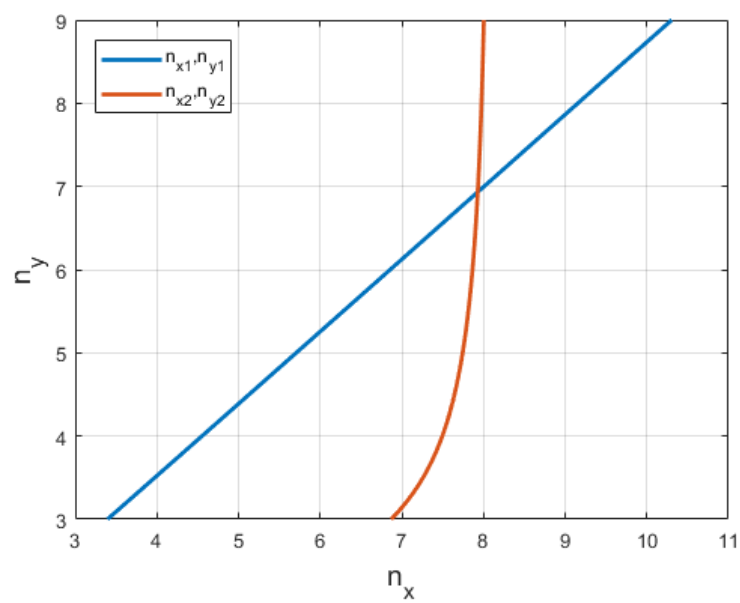

Figure 4.4 (a): Solution space for n_x and n_y when $HPBW_x^{(1)} = 7.5°$, $HPBW_y^{(1)} = 9.5°, SLL^{(1)} = -40$ dB and $\theta_0 = 25, \phi_0 = 90°$

1	3	6	10	15	21	28	36	42	46	48	48	46	42	36	28	21	15	10	6	3	1
3	9	18	30	45	63	84	108	126	138	144	144	138	126	108	84	63	45	30	18	9	3
6	18	36	60	90	126	168	216	252	276	288	288	276	252	216	168	126	90	60	36	18	6
10	30	60	100	150	210	280	360	420	460	480	480	460	420	360	280	210	150	100	60	30	10
15	45	90	150	225	315	420	540	630	690	720	720	690	630	540	420	315	225	150	90	45	15
21	63	126	210	315	441	588	756	882	966	1008	1008	966	882	756	588	441	315	210	126	63	21
28	84	168	280	420	588	784	1008	1176	1288	1344	1344	1288	1176	1008	784	588	420	280	168	84	28
33	99	198	330	495	693	924	1188	1386	1518	1584	1584	1518	1386	1188	924	693	495	330	198	99	33
36	108	216	360	540	756	1008	1296	1512	1656	1728	1728	1656	1512	1296	1008	756	540	360	216	108	36
37	111	222	370	555	777	1036	1332	1554	1702	1776	1776	1702	1554	1332	1036	777	555	370	222	111	37
36	108	216	360	540	756	1008	1296	1512	1656	1728	1728	1656	1512	1296	1008	756	540	360	216	108	36
33	99	198	330	495	693	924	1188	1386	1518	1584	1584	1518	1386	1188	924	693	495	330	198	99	33
28	84	168	280	420	588	784	1008	1176	1288	1344	1344	1288	1176	1008	784	588	420	280	168	84	28
21	63	126	210	315	441	588	756	882	966	1008	1008	966	882	756	588	441	315	210	126	63	21
15	45	90	150	225	315	420	540	630	690	720	720	690	630	540	420	315	225	150	90	45	15
10	30	60	100	150	210	280	360	420	460	480	480	460	420	360	280	210	150	100	60	30	10
6	18	36	60	90	126	168	216	252	276	288	288	276	252	216	168	126	90	60	36	18	6
3	9	18	30	45	63	84	108	126	138	144	144	138	126	108	84	63	45	30	18	9	3
1	3	6	10	15	21	28	36	42	46	48	48	46	42	36	28	21	15	10	6	3	1

Figure 4.4 (b): Current distribution of the designed array when $n_x = 8, n_y = 7$ and $m = 3$

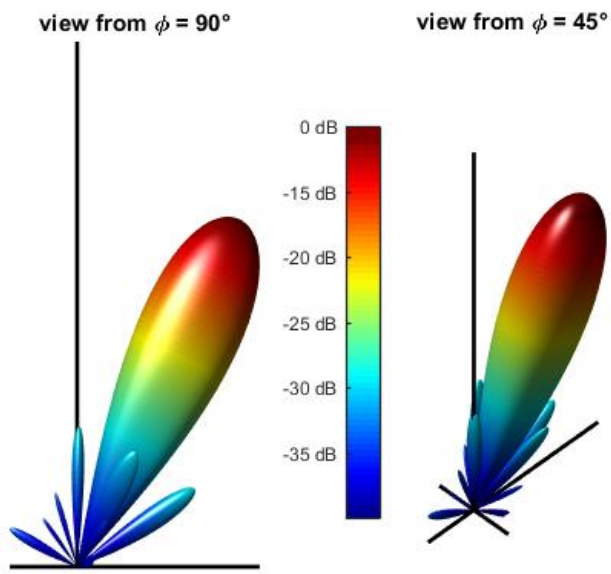

Figure 4.4 (c): Radiation Pattern of the designed array when $n_x = 8, n_y = 7$ and $m = 3$

Table 4.4: Comparison of design requirements with achieved characteristics

$HPBW_x^{(1)}$	$HPBW_x^{(2)}$	$HPBW_y^{(1)}$	$HPBW_y^{(2)}$	$SLL^{(1)}$[dB]	$SLL^{(2)}$[dB]
7.5°	7.56°	9.5°	9.57°	−40	−38

Chapter 5: Conclusions and Suggestions for Future Work

A new class of low side lobe planar arrays (LSPA) has been proposed and examined in this study. These new arrays lend themselves to analytical formulation of radiation properties, thus allowing their analysis and synthesis to be carried out more efficiently and rapidly. The main objective of the research has two parts: i) Define, develop and study analytical expressions for half-power beamwidths, side lobe level, and the array excitation coefficients, and ii) Use the analytical expressions as design equations to synthesize arrays for any given radiation pattern requirements. A summary of important attributes of the proposed array and its performance are presented below. The main contributions of the research are highlighted and potential scope for future work is also identified.

5.1 Summary

5.1.1 Development of Analytical Results

The array factor of the LSPA was defined as the mth power of the array factor of a uniformly excited rectangular array of $n_x \times n_y$ elements. It was found that, under certain constraints, the larger side lobe level of the constituent low side lobe linear arrays (LSLA) is also the side lobe level of the planar array. Thus, the procedure for calculation of the side lobe level of LSLA was extended to the planar array case.

Two half-power beamwidths for LSPA were defined in *x*-*r* and *y*-*r* planes considered as principal planes, where the *x*-*r* plane comprises the *x* axis and the radial line *r* going through the origin and along the direction of main beam maximum radiation, and the *y*-*r* plane included the *y* axis and the same *r* line as defined above. Assuming that half-power points on the above two planes are in the visible range, analytical expressions for half-power beamwidths were developed.

The calculation procedure for element excitation coefficients used for LSLA was extended in this study to determine excitation coefficients of LSPA. This was possible due to the fact that the proposed planar array has a separable element current distribution. The excitation

of the pq^{th} element of the planar array was found to be the product of pth and q^{th} element excitations of the constituent LSLA arrays.

5.1.2 Analysis of Directivity, SLL and HPBW

The developed results were used to analyze the directivity of planar arrays. For a fixed size LSPA, the best directivity performance was observed for the broadside case with the maximum radiation on the main beam occurring along the normal to the plane of the array. Steering the main lobe away from the broadside direction resulted in beam broadening, and consequently reduction of directivity. It was also observed that when the main lobe was steered in the azimuthal direction variations in half-power beamwidths and directivity were negligible for small elevation angles of boresight and more pronounced at higher elevation angles. Furthermore, for large arrays, unlike Chebyshev arrays, no directivity saturation was noticed.

The SLL of the proposed planar array is always smaller than that of a uniformly excited rectangular array of equal size. It was further noted that for a fixed value of parameter *m*, increasing either N_x or N_y alone caused SLL to decrease initially and then saturate to a certain value, but this saturation does not occur when N_x or N_y is increased by increasing *m*, while keeping n_x and n_y constant.

Finally, it was noted that the maximum excitation amplitude belongs to the element located at the array center of the array when both N_x and N_y are odd, or otherwise to the elements in the immediate neighborhood of the center. The excitation amplitudes decreased monotonically from the center of the array to its corner elements. Furthermore, symmetry of the array with respect to two lines parallel to *x*- and *y*-axes and passing through the array center made it mathematically easier to compute the excitation amplitudes of the array by just determining the element currents for about one quarter of the elements.

5.1.3 Synthesis of LSPA

The equations governing HPBW and SLL can also be used to synthesize low side lobe, non-uniformly excited planar arrays for given radiation pattern requirements. The array synthesis was achieved by developing new design equations based on the existing

relationships used for the evaluation of $HPBW_x, HPBW_y$ and SLL. The design parameters are n_x, n_y and m which are determined for known values of half-power beamwidths and side lobe level. Once these parameters are found, the total number of array elements and element excitation coefficients were readily calculated. The radiation characteristics of the designed array were found to be very close to the required values.

5.2 Contributions

A low side lobe array synthesis procedure has been proposed and verified by implementing it to design planar arrays of isotropic elements. The main contributions of this research are summarized as follows:

- The proposed synthesis method is analytically convenient to implement and circumvents the issue of implementing complex and time consuming optimization algorithms to achieve desired radiation pattern requirements.
- The analytical synthesis technique proposed in this study provides a much more robust control over the design procedure, making it more useful when analyzing main lobe properties for important applications involving e.g. beam steering
- Using the synthesis procedure, low side lobe planar arrays were designed with reasonable accuracies.
- The literature only deals with HPBW calculation of planar arrays for broadside case and few analytical procedures have so far dealt with tracking main lobe variations when it is not in the broadside direction. In that regard, the proposed HPBW calculation procedure in this study provides a new framework to analyze beam broadening and narrowing in planar arrays.

5.3 Suggestions for Future Work

A number of questions require further investigation when analyzing and designing arrays using the procedure proposed in this research. They are summarized as follows

- For LSPA with large number of elements, the issue of limiting the current taper ratio without adversely impacting the desired performance still remains to be analyzed.

- The design challenges in practical implementation of the array requires careful selection of antenna type to achieve the array configuration and its overall performance. In that regard, the effect of mutual coupling between the antenna elements needs to be accounted for.

References

[1] L. C. Godara, "Applications of antenna arrays to mobile communications. I. Performance improvement, feasibility, and system considerations," in *Proceedings of the IEEE*, vol. 85, no. 7, pp. 1031-1060, Jul 1997.

[2] O. H. Koymen, A. Partyka, S. Subramanian and J. Li, "Indoor mm-Wave Channel Measurements: Comparative Study of 2.9 GHz and 29 GHz," *2015 IEEE Global Communications Conference (GLOBECOM)*, San Diego, CA, 2015, pp. 1-6.

[3] J. Zhang, X. Ge, Q. Li, M. Guizani and Y. Zhang, "5G Millimeter-Wave Antenna Array: Design and Challenges," in *IEEE Wireless Communications*, vol. 24, no. 2, pp. 106-112, April 2017.

[4] M. Y. Li, Y. L. Ban, Z. Q. Xu, J. Guo and Z. F. Yu, "Tri-Polarized 12-Antenna MIMO Array for Future 5G Smartphone Applications," in *IEEE Access*, vol. PP, no. 99, pp. 1-1.

[5] S. Ye *et al*., "High-Gain Planar Antenna Arrays for Mobile Satellite Communications [Antenna Applications Corner]," in *IEEE Antennas and Propagation Magazine*, vol. 54, no. 6, pp. 256-268, December 2012.

[6] E. Alles, N. Fook Sheung, S. Noimark, E. Zhang, P. Beard and A. Desjardins, "A reconfigurable all-optical ultrasound transducer array for 3D endoscopic imaging", *Scientific Reports*, vol. 7, no. 1, 2017.

[7] G. Oliveri, M. Carlin and A. Massa, "Synthesis of planar arrays through Bayesian Compressive Sensing," *Proceedings of the 2012 IEEE International Symposium on Antennas and Propagation*, Chicago, IL, 2012, pp. 1-2.

[8] R. Harrington, "Sidelobe reduction by nonuniform element spacing," in *IRE Transactions on Antennas and Propagation*, vol. 9, no. 2, pp. 187-192, March 1961.

[9] V. Murino, A. Trucco and C. S. Regazzoni, "Synthesis of unequally spaced arrays by simulated annealing," in *IEEE Transactions on Signal Processing*, vol. 44, no. 1, pp. 119-122, Jan 1996.

[10] Bin Sun, Shiqi Xing, Jingke Zhang, F. Li, Yongzhen Li and Xuesong Wang, "A novel sparse array synthesis method based on two-step convex optimization," *2016 10th European Conference on Antennas and Propagation (EuCAP)*, Davos, 2016, pp. 1-3.

[11] G. Toso, C. Mangenot and A. G. Roederer, "Sparse and Thinned Arrays for Multiple Beam Satellite Applications," *The Second European Conference on Antennas and Propagation, EuCAP 2007*, Edinburgh, 2007, pp. 1-4.

[12] F. T. Bendimerad, E. Cambiaggio and A. Papiernik, "Synthesis of uniformly excited non-periodic antenna arrays: application to microstrip antennas," *1988 IEEE AP-S. International Symposium, Antennas and Propagation*, Syracuse, NY, USA, 1988, pp. 462-465 vol.2.

[13] D. K. Cheng, "Optimization techniques for antenna arrays," in *Proceedings of the IEEE*, vol. 59, no. 12, pp. 1664-1674, Dec. 1971.

[14] R. L. Haupt, J. J. Menozzi and C. J. McCormack, "Thinned arrays using genetic algorithms," Proceedings of IEEE Antennas and Propagation Society International Symposium, Ann Arbor, MI, USA, 1993, pp. 712-715 vol.2.

[15] A. Trucco, "Thinning and weighting of large planar arrays by simulated annealing," in *IEEE Transactions on Ultrasonics, Ferroelectrics, and Frequency Control*, vol. 46, no. 2, pp. 347-355, March 1999.

[16] J. F. DeFord and O. P. Gandhi, "Phase-only synthesis of minimum peak sidelobe patterns for linear and planar arrays," in *IEEE Transactions on Antennas and Propagation*, vol. 36, no. 2, pp. 191-201, Feb 1988.

[17] R. E. Hodges and Y. Rahmat-Samii, "On sampling continuous aperture distributions for discrete planar arrays," in *IEEE Transactions on Antennas and Propagation*, vol. 44, no. 11, pp. 1499-1508, Nov 1996.

[18] W. H. Kummer, "Basic array theory," in *Proceedings of the IEEE*, vol. 80, no. 1, pp. 127-140, Jan 1992.

[19] Y. V. Baklanov, “Chebyshev distribution of currents for a plane array of radiators,” *Radio Engineering and Electronic Physics*, Vol. 11, pp. 640-642, April 1966.

[20] Fung-I Tseng and D. K. Cheng, "Optimum scannable planar arrays with an invariant sidelobe level," in *Proceedings of the IEEE*, vol. 56, no. 11, pp. 1771-1778, Nov. 1968.

[21] R.E. Collin and . J. Zucker (Ed), *Antenna Theory, Part 1*, McGraw Hill, New York, 1969

[22] K. Y. Kabalan, A. El-Hajj and M. Al-Husseini, "Modified Chebyshev planar arrays," in Radio Science, vol. 37, no. 5, pp. 1-9, Oct. 2002.

[23] K. Y. Kabalan, A. El-Hajj and M. Al-Husseini, "Bessel planar arrays," in *Radio Science*, vol. 39, no. 1, pp. 1-9, Feb. 2004.

[24] A. Safaai-Jazi and W. L. Stutzman, "A New Low-Sidelobe Pattern Synthesis Technique for Equally Spaced Linear Arrays," in *IEEE Transactions on Antennas and Propagation*, vol. 64, no. 4, pp. 1317-1324, April 2016.

[25] Robert S. Elliot, Antenna Theory and Design, Wiley-IEEE Press, January 2003, pp. 197-210.

[26] IEEE Standard for Definitions of Terms for Antennas," in *IEEE Std 145-2013 (Revision of IEEE Std 145-1993)* , vol., no., pp.1-50, March 6 2014

[27] W. L. Stutzman, G. A. Thiele, Antenna Theory and Design, Hoboken, NJ, USA:Wiley, pp. 2013.

[28] A. Safaai-Jazi and W. L. Stutzman, "Synthesis of low side lobe planar arrays," *2016 IEEE International Symposium on Antennas and Propagation (APSURSI)*, Fajardo, 2016, pp. 1873-1874